Secondary Organic Aerosol Formation from Nitrate Radical Oxidation of Styrene: Aerosol Yields, Chemical Composition, and Hydrolysis of Organic Nitrates

Yuchen Wang[1,2], Xiang Zhang[1], Yuanlong Huang[3], Yutong Liang[2,6], Nga L. Ng*[,2,4,5]

[1] College of Environmental Science and Engineering, Hunan University, Changsha, Hunan, 410082, China
[2] School of Chemical and Bimolecular Engineering, Georgia Institute of Technology, Atlanta, Georgia 30332, USA
[3] Ningbo Institute of Digital Twin, Eastern Institute of Technology, Ningbo, 315200, China
[4] School of Civil and Environmental Engineering, Georgia Institute of Technology, Atlanta, Georgia 30332, USA
[5] School of Earth and Atmospheric Sciences, Georgia Institute of Technology, Atlanta, Georgia 30332, USA
[6] Thrust of Sustainable Energy and Environment, The Hong Kong University of Science and Technology (Guangzhou), Guangdong, 511453, China
*Corresponding Author: Nga L. Ng (ng@chbe.gatech.edu)

Abstract

Styrene is emitted from anthropogenic sources and biomass burning and is highly reactive towards atmospheric oxidants. While it has the highest nitrate radical (NO_3) reactivity among aromatic hydrocarbons, the NO_3 oxidation of styrene and formation mechanisms of secondary organic aerosols (SOA) have not been investigated. In this study, we conduct chamber experiments with styrene concentrations ranging from 9.5-155.2 ppb. The resulting SOA yields range from 14.0-22.1% with the aerosol mass loadings of 5.9-147.6 μg m^{-3} after wall loss corrections. The chemical composition of SOA is characterized by online measurements, revealing that dimeric organic nitrates (ONs) constitute 90.9% of the total signal of particle-phase products. $C_{16}H_{16}N_2O_8$ and $C_8H_9NO_4$ are identified as the major particle-phase products, which constitute 88.3% and 4.1% of the measured signal, respectively. We propose formation mechanisms for the ON products, including the common RO_2+RO_2/HO_2 pathway and other radical chain termination reactions such as RO+R and R+R. We also investigate the hydrolysis of particulate ONs. The hydrolysis lifetime for ONs is determined to be less than 30 minutes. This short hydrolysis lifetime can be attributed to the stabilization of the carbocation by delocalized π orbitals of the benzene-related skeleton of aromatic ONs. This work provides the first fundamental laboratory data to evaluate SOA production from styrene+NO_3 chemistry. Additionally, the formation mechanisms of aromatic ONs are reported for the first time, highlighting that compounds previously identified as nitroaromatics in ambient field campaigns could also be attributed to aromatic ONs.

1. Introduction

Aromatic hydrocarbons are a class of unsaturated chemical compounds characterized by the presence

of delocalized π orbitals. They play a crucial role in the atmosphere, contributing up to 60% of volatile organic compounds (VOCs) in urban environments (Calvert et al., 2002; Cabrera-Perez et al., 2016). Styrene is particularly unique within aromatic hydrocarbons as it possesses both an unsaturated double bond and a benzene ring and has the combined properties of alkenes and aromatic compounds. Although styrene is not the most abundant aromatic hydrocarbon, with concentrations ranging from 0.06 to 45 ppb in the atmosphere (Cho et al., 2014; Tuazon et al., 1993), it has the highest reaction rate constants for reactions with hydroxyl radicals (OH), nitrate radicals (NO_3), ozone (O_3), and chlorine radicals because of the unsaturated double bond (Tuazon et al., 1993; Tajuelo et al., 2019a, b; Atkinson and Aschmann, 1988; Le Person et al., 2008; Cho et al., 2014). In addition, styrene is the second most efficient aromatic hydrocarbon in forming secondary organic aerosols (SOA) during daytime chemistry, surpassed only by toluene (Sun et al., 2016). SOA yields from OH-initiated photooxidation of styrene can reach as high as around 35% for an aerosol mass loading of 430 $\mu g/m^3$ (Schueneman et al., 2024). A theoretical study suggests that OH-initiated photooxidation of styrene could be a substantial contributor to SOA formation in urban environments (Wang et al., 2015).

To the best of our knowledge, no study has specifically investigated SOA formation from styrene+NO_3 oxidation. Although styrene emissions from various anthropogenic sources such as industrial activities, motor vehicle operations, combustion processes, building materials, or consumer products (Zhang et al., 2017; Knighton et al., 2012; Helal and Elshafy, 2012; Okada et al., 2012), are predominantly active during the daytime, high levels of styrene have also been observed at night in urban environments. The nighttime presence of styrene is likely influenced by the boundary layer accumulation effect (Wu et al., 2020; Lu et al., 2023a), which enhances the conditions for styrene+NO_3 oxidation. Additionally, biomass burning, particularly wildfires, contributes to emission of styrene in rural and forest regions (Koss et al., 2018). The NO_3 oxidation of styrene can occur under conditions such as nighttime chemistry or optically dense plumes during biomass burning events (Decker et al., 2021). Given that styrene exhibits the highest NO_3 reactivity among aromatic hydrocarbons (Yang et al., 2020), the styrene+NO_3 oxidation can play a major role in the consumption of styrene and formation of SOA.

The NO_3 oxidation of VOCs is also expected to generate a substantial quantity of organic nitrates (ONs), primarily through the direct incorporation of the NO_3 with the double bond during reactions (Ng et al., 2017; Orel et al., 1978). ONs have been shown to influence NO_x recycling, O_3 production, and the formation of SOA in the atmosphere (Ng et al., 2017). Ambient field measurements consistently demonstrate the widespread presence of ONs derived from aromatics in submicron organic aerosols at various locations globally (Lu et al., 2023b; Lin et al., 2021; Jiang et al., 2023; Yang et al., 2019). For example, in Shanghai, around 16% of the oxygenated organic molecules containing two nitrogen atoms originate from aromatic compounds (Lu et al., 2023b). In Beijing, the concentration of phenethyl nitrate is

found to be 3.23 ng m^{-3} (Yang et al., 2019). All these suggest that the oxidation of styrene by NO_3 could be an important pathway for generating aromatic ONs.

Hydrolysis of particulate ONs is an important sink of NO_x, especially when the ONs have short hydrolysis lifetimes (Pye et al., 2015; Fisher et al., 2016; Zare et al., 2019; Vasquez et al., 2021; Takeuchi and Ng, 2019). To our knowledge, there is only one study on hydrolysis of ONs formed from oxidation of 1,2,4-trimethylbenzene (Liu et al., 2012). More studies focus on biogenic ONs. For instance, results from hydrolysis of biogenic ONs in bulk solutions indicate that the number of alkyl substitutions, the types of functional groups, and the structures of carbon skeletons are three important factors controlling hydrolysis rates (Darer et al., 2011; Hu et al., 2011; Jacobs et al., 2014; Rindelaub et al., 2016; Wang et al., 2021b). A common feature identified in the mechanisms is the formation of stable carbocations, which facilitates the rapid hydrolysis of ONs. Previous research indicates that the benzene-related skeleton, featuring three delocalized π orbitals, enhances the hyper-conjugation effect and stabilizes the carbocation (Wang et al., 2021b). Consequently, ONs produced from styrene+NO_3 oxidation, which include such benzene-related skeletons, are likely to have short hydrolysis lifetimes. However, this hypothesis has not been evaluated before, because of the lack of hydrolysis studies of aromatic ONs.

In this study, we aim to investigate SOA formation and chemical composition from styrene+NO_3 oxidation. We conduct a series of chamber experiments in the dark under both dry and humid conditions. SOA yields are determined across a wide range of initial styrene concentrations under dry conditions. The chemical composition of SOA is characterized by online mass spectrometry and the SOA formation mechanism is proposed based on these measurements. Additionally, we investigate hydrolysis of particulate ONs. These results can be used to estimate SOA formation and transformation from NO_3 oxidation of styrene from anthropogenic emissions and biomass burning in ambient environments.

2. Experimental Section

2.1. Environmental chamber experiments

The experimental conditions are summarized in Table 1. All experiments are performed in the Georgia Tech Environmental Chamber (GTEC) Facility, which consists of two 12 m^3 Teflon chambers (Boyd et al., 2015). Experiments are conducted at 295 ± 3 K and ambient pressure. Most experiments are conducted under dry conditions (RH < 3%, Exp. 1-10), with the exception of two experiments (Exp. 11 and 12), which are conducted under humid conditions (approximately 50% and 70%, respectively). These humid experiments allow for the investigation of the hydrolysis processes of SOA.

A typical experiment begins with the injection of seed particles into the chamber by atomizing a dilute ammonium sulfate solution (AS; 0.015 M). Subsequently, styrene (99 %, Sigma-Aldrich) is injected into the chamber using a glass bulb, where the evaporation of styrene is facilitated by the flow of zero air at a rate of 5 L min^{-1} through the bulb. The initial particle number and volume concentration are 2.9×10^4

particles cm^{-3} and 3.2×10^{10} nm^3 cm^{-3}, respectively. The initial concentration of styrene ranges from 9.5-155.2 ppb. It is noted that Exp. 9 and 10 do not involve seed particle injection and are conducted specifically to determine the density of styrene+NO_3 SOA.

N_2O_5 is generated by the reaction of NO_2 (Matheson, 500 ppm) and O_3 (generated by passing purified air through a UV light (Jelight 610), ~125 ppm) in a flow tube (0.8 L min^{-1} flow rate, 115 s residence time) and injected into the chamber as NO_3 precursor, similar to our prior studies (Boyd et al., 2017; Takeuchi and Ng, 2019; Takeuchi et al., 2022). The injection time ranges from 5 to 75 minutes, depending on the initiation concentration of styrene. The typical styrene to N_2O_5 ratio is approximately 1:2. To ensure that styrene is predominantly oxidized by NO_3, the concentrations of O_3 and the flow rates of both NO_2 and O_3 are adjusted (based on results from a simple kinetic box model, Table S1) to optimize N_2O_5 production while minimizing O_3 concentration. Upon entering the chamber, N_2O_5 thermally decomposes, generating NO_2 and NO_3, establishing an equilibrium that marks the onset of NO_3 oxidation (Boyd et al., 2015; Takeuchi and Ng, 2019).

2.2. Gas- and particle-phase measurements

The concentrations of O_3 and NO_x are monitored with an ultraviolet absorption O_3 monitor (Teledyne T400) and a NO_x monitor (Thermo Fisher Scientific 42C) (Teledyne 200EU), respectively. A gas chromatograph with flame ionization detector (GC-FID, Agilent) is used to track the decay of styrene. Aerosol volume and size distributions of particles smaller than 1 μm in electrical mobility diameter are measured by a scanning mobility particle sizer (SMPS) under the low-flow mode (sheath flow of 2 L min^{-1}). The SMPS is consisted with a differential mobility analyzer (TSI 3080) and a condensation particle counter (TSI 3775).

A high-resolution time-of-flight aerosol mass spectrometer (HR-ToF-AMS; Aerodyne Research Inc.) is used to quantitatively measure the bulk particle-phase chemical composition including organics, nitrate, sulfate, ammonium, and chloride. The working principle and operation of the HR-ToF-AMS are described in detail elsewhere (DeCarlo et al., 2006). Elemental analysis of the data is conducted to determine the elemental composition of the bulk aerosols (Canagaratna et al., 2015). The data are analyzed using PIKA v1.16I in Igor Pro 6.38B.

The speciated oxidized gas- and particle-phase products are measured using a high-resolution time-of-flight chemical-ionization mass spectrometer coupled with the filter inlet for gases and aerosols (FIGAERO-CIMS; Aerodyne Research Inc.) with iodide (I^-) as the reagent ion. Details on the operation of the instrument has been described in previous literature (Boyd et al., 2017; Takeuchi and Ng, 2019; Nah et al., 2016b; Chen et al., 2020; Lopez-Hilfiker et al., 2014). Briefly, reagent ions are generated from a cylinder containing a mixture of CH_3I and dry N_2 (Airgas) and through polonium-210 source (NRD; model P-2021). Each sampling cycle lasts for 60 minutes. The instrument measures gaseous compounds by sampling air from

the chamber at 1.7 L min^{-1} for 30 minutes. At the same time, particles in the chamber are collected onto a polytetrafluoroethylene filter with the sampling rate from 1 to 5 L min^{-1} depending on the aerosol mass concentrations. A gradually heated nitrogen gas flows over the filter, evaporating oxidized organic species and transporting them into the CIMS for detection, with a temperature ramp period of 10 minutes, a soak period of 15 minutes, and a cooling phase of 5 minutes. The data are analyzed using Tofware v2.5.11. All the compounds presented in this study are I^- adducts.

2.3. Volatility Calibration

In the FIGAERO-CIMS, during the thermal desorption stage, the temperature at which the maximum (T_{max}) desorption signal for a particle-phase compound is observed corresponds to effective saturation mass concentration (C*) (Lopez-Hilfiker et al., 2014; Thornton et al., 2020; Stark et al., 2017; Ylisirniö et al., 2021). The experimental procedures for volatility calibration have been described in detail in our previous study (Takeuchi et al., 2022). Briefly, the relationship between T_{max} and C* in FIGAERO-CIMS is established by depositing a mixture of standards with known C* onto the filter. These standards are then subjected to thermal desorption using the same thermal program applied in the chamber experiments. The standards used in this study include glycolic acid ($C_2H_4O_3$), oxalic acid ($C_2H_4O_2$), malonic acid ($C_3H_3O_4$), succinic acid ($C_4H_6O_4$), meso-erythritol ($C_4H_{10}O_4$), levoglucosan ($C_6H_{10}O_5$), suberic acid ($C_8H_{14}O_4$), azelaic acid ($C_9H_{16}O_4$), sebacic acid ($C_{10}H_{18}O_4$), dodecanedioic acid ($C_{12}H_{22}O_4$), palmitic acid ($C_{16}H_{32}O_2$), stearic acid ($C_{18}H_{36}O_2$), and behenic acid ($C_{22}H_{44}O_2$). The relationship between C* (in μg m^{-3}) at 25 ˚C and T_{max} (in ˚C) obtained in this study is $\log_{10}[C^*_{25^\circ C}] = -0.085T_{max} + 5.12$ (Figure S1) and is consistent with the calibrations in Takeuchi et al. (2022).

3. Results

3.1. SOA formation from NO_3 radical oxidation of styrene

A series of chamber experiments with different initial styrene concentrations is performed to investigate SOA formation from NO_3 oxidation of styrene (Table 1). In these experiments, the ratio of styrene to N_2O_5 is maintained at 1:2 to optimize the reaction conditions, facilitating a complete consumption of styrene and allowing for the analysis of the resulting products. Figure S2 presents the time series of the formation of SOA during a typical experiment (Exp. 7). In all experiments, styrene is fully reacted within 60 minutes, and the peak aerosol concentration is typically observed within the same time range (Figure S2).

All SOA data are corrected for particle wall loss by applying size-dependent coefficients determined from wall loss experiments (Nah et al., 2017). The nucleation experiments are conducted to determine SOA density. By comparing SMPS volume distribution and HR-ToF-AMS mass distribution (Bahreini et al., 2005; Alfarra et al., 2006; Ng et al., 2008), the SOA density is determined to be 1.35 ± 0.1 g cm^{-3}. Figure 1 shows the SOA yields (Y, 4.5%–16.1% for Exp. 1-8, over a wide range of aerosol mass loadings (ΔM_O),

1.9–107.4 μg/m^3). For all experiments, peak aerosol mass concentration is obtained from the SMPS aerosol volume concentration (averaged over 30 minutes at peak aerosol loading) and the calculated aerosol density. SOA yields are parametrized as a function of organic mass produced using the a semi-empirical model (Odum et al., 1996, 1997) based on gas-to-particle partitioning of two semi-volatile products (Eq.1). The fitting molar yields (α_1 and α_2) are 0.1 and 0.09, and the fitted partitioning coefficients (K_1 and K_2) are 0.4 and 0.02 (R^2 = 0.997).

$$Y = \Delta M_O \left[\frac{\alpha_1 K_1}{1+K_1 M_O} + \frac{\alpha_2 K_2}{1+K_2 M_O}\right] \quad \text{Eq. 1}$$

3.2. Chemical composition of SOA

A typical HR-ToF-AMS aerosol mass spectrum is shown in Figure 2 along with the National Institute of Standards and Technology (NIST) mass spectra of possible styrene+NO_3 oxidation products. There are a few notable ions in the aerosol mass spectrum. The signals at *m/z* 39 ($C_3H_3^+$), 50 ($C_4H_2^+$), 51 ($C_4H_3^+$), 52 ($C_4H_4^+$), 77 ($C_6H_5^+$), 78 ($C_6H_6^+$), 91 ($C_7H_7^+$), 105 ($C_7H_5O^+$), and 106 ($C_7H_6O^+$) are aromatic compound signatures with benzene ring (McLafferty and Turecek, 1993). The signals at *m/z* 91 ($C_7H_7^+$), 105 ($C_7H_5O^+$), and 106 ($C_7H_6O^+$), while not particularly significant in the mass spectra of other aromatic SOA systems (Yu et al., 2014, 2016; Zhang et al., 2023; Liu et al., 2022; Chen et al., 2021), are relatively high for styrene+NO_3 oxidation system. However, *m/z* 91 ($C_7H_7^+$) is a signature ion for SOA formed from NO_3 oxidation of β-pinene (Boyd et al., 2015) and photooxidation of β-caryophyllene (Tasoglou and Pandis, 2015). *m/z* 91 ($C_7H_7^+$) has also been detected as one of the major fragments of synthetic monoterpene ON standards measured by HR-ToF-AMS (Takeuchi et al., 2024). Therefore, only *m/z* 105 ($C_7H_5O^+$) and 106 ($C_7H_6O^+$) can potentially serve as useful indicators for SOA formed from styrene oxidation in ambient aerosol mass spectra. Note that the HR-ToF-AMS spectrum of styrene+NO_3 oxidation is very similar to the NIST mass spectra of benzaldehyde (C_7H_6O) and 2-hydroxy-1-phenyl ethanone ($C_8H_8O_2$). However, we do not detect the prominent peaks of dimers in the HR-ToF-AMS, which can be explained by instability of dimer under the high collision energy of the instrument.

Figure S3a presents the time series of organics and nitrate as measured by HR-ToF-AMS from a typical experiment. Sulfate is used to normalize the decay of organics and nitrate because it is non-volatile and any decrease in sulfate is reflective of particle wall loss and changes in aerosol collection efficiency (CE) in the HR-ToF-AMS (Henry and Donahue, 2012). Organics and nitrate exhibit similar decay trends. However, the situation differs when examining the time series of major organic families relative to sulfate (Figure S3b). Hydrocarbon fragments (C_xH_y Family), C_xH_yO family, and $C_xH_yO_zN$ (z>1) family exhibit similar decay rates, but decrease more rapidly relative to sulfate than C_xH_yON and $C_xH_yO_z$ families. This may indicate that further aerosol aging leads to the formation of more oxidized fragments ($C_xH_yO_z$) (Boyd et al., 2015). This may also suggest that the aging products are more likely to produce C_xH_yON rather than $C_xH_yO_zN$

fragments.

FIGAERO-CIMS is used to measure speciated particle-phase composition of styrene+NO_3 SOA, including both dimeric and monomeric products. The characteristic SOA mass spectrum from FIGAERO-CIMS (Figure 3a) is categorized according to molecule types: CHO, CHON, and $CHON_2$, each contains compounds with different numbers of carbon atoms (Figure 3b). The SOA composition is dominated by nitrogen-containing compounds, with $C_xH_yO_zN_2$, $C_xH_yO_zN$, and $C_xH_yO_z$ molecules constituting 91.8%, 7.4%, and 0.8% of the measured signal, respectively (Figure 3c). Dimers (with carbon numbers C_9 to C_{16}) make up 90.9% of the signal, with the majority being $C_{16}H_xO_zN_2$ dimers constituting 89.4% of the total signal. The relative percentage contributions of CHO, CHON, $CHON_2$, as well as dimers and monomers, remained relatively stable across various experiments with differing initial styrene concentrations (Figure S4). Figure 4 shows the temporal evolution of major particle-phase products, the dominant product is $C_{16}H_{16}N_2O_8$, contributing 88.3% of the total signal. The next most abundant particle-phase product is $C_8H_9NO_4$, which constitutes 4.1% of the total signal. In addition, $C_8H_7NO_4$, $C_8H_9NO_5$, $C_8H_8N_2O_6$, and $C_8H_8N_2O_7$ are major monomeric particle-phase products. $C_{16}H_{14}N_2O_8$, $C_{16}H_{17}NO_7$, $C_{15}H_{13}NO_6$, and $C_{16}H_{13}NO_6$ are major dimeric particle-phase products. It is noted that it is possible that the compounds detected as monomeric species are formed from the thermal decomposition process in the FIGAERO-CIMS (Yang et al., 2021; Kumar et al., 2023; Stark et al., 2017).

3.3. Hydrolysis of styrene-derived organic nitrates

Building on results from our previous study (Wang et al., 2021b), the unique benzene-related skeleton of styrene ONs can facilitate their rapid hydrolysis. Therefore, we conduct experiments with three different chamber RH, including dry (RH<3%), RH~50%, and RH~70% to study the hydrolysis of styrene-derived ONs. Figure S5 illustrates the time series of nitrate measured by HR-ToF-AMS for these different RH systems. Distinct variations are observed in nitrate levels across different chamber RH conditions. The presence of the small amounts of nitrate prior to the commencement of experiments under different RH conditions could potentially result from the uptake of background nitric acid onto aqueous seed particles (McMurry and Grosjean, 1985; Grosjean, 1985; Matsunaga and Ziemann, 2010; Zhang et al., 2014, 2015; Yeh and Ziemann, 2015; La et al., 2016; Nah et al., 2016a; Krechmer et al., 2016; Huang et al., 2018). After N_2O_5 is injected into the chamber, the large increase in nitrate in the higher RH experiments can be attributed to the reactive uptake of N_2O_5 and/or the dissolution of HNO_3 into aqueous aerosols (Takeuchi and Ng, 2019), subsequently neutralized by ammonia to form ammonium nitrate. Therefore, to evaluate the extent of particle phase ONs hydrolysis, the contributions of inorganic nitrate ($NO_{3,Inorg}$) and ONs ($NO_{3,Org}$) to the measured nitrate from HR-ToF-AMS need to be separated.

We differentiate the contributions of $NO_{3,Inorg}$ and $NO_{3,Org}$ to the measured nitrate based on the method reported in Farmer et al., (2010), as described in Eq. 2.

$$x = \frac{(R_{obs} - R_{NH_4NO_3})(1+R_{ON})}{(R_{ON} - R_{NH_4NO_3})(1+R_{obs})} \quad \text{Eq. 2}$$

Where R_{NH4NO3} (*i.e.*, NO^+/ NO_2^+ from ammonium nitrate) is derived from the standard ionization efficiency (IE) calibration of HR-ToF-AMS using 300 nm-sized ammonium nitrate particles, and the value is 1.8. The R_{ON} (*i.e.*, NO^+/ NO_2^+ for ONs) value is dependent on the aerosol chemical composition and instrument. The NO^+/ NO_2^+ ratio throughout all the dry experiments remains constant at approximately 4.9, referred to as R_{ON} in this study. The R_{ON}/R_{NH4NO3} ratio (ratio of ratio, RoR) is 2.7, which falls within the range of previous studies with the presence of ONs (Day et al., 2022). The R_{obs} value is 2.8 and 3.8 for experiments with RH ~70% and 50%, corresponding to $NO_{3,Org}$ contributions of 51% and 80%, respectively. Figures S5b and S6 depict the time series of $NO_{3,Org}$ for experiments under different RH. We also compare the $NO_{3,Org}$ measured by HR-ToF-AMS and speciated ONs measured by FIGAERO-CIMS, which show similar trends (Figure S6).

Here, we follow the approach reported in our previous work and used $_pON/OA$ ratio to evaluate the extent of ON hydrolysis via Eq. 3 (Takeuchi and Ng, 2019; Takeuchi et al., 2024). It is noted that $_pON$ refers to the total mass concentration of particulate ONs, encompassing both the organic and nitrate components of the ON compounds. Similarly, OA represents the total mass concentration of organic aerosols, which includes both nitrated and non-nitrated organic compounds.

$$\frac{_pON}{OA} = \left(\frac{NO_{3,org}}{Organic + NO_{3.org}}\right) \times \left(\frac{MW_{\ _pON}}{MW_{NO_{2,ON}}}\right) = \left(\frac{\frac{NO_{3,org}}{Organic}}{1+\frac{NO_{3,Org}}{Organic}}\right) \times \left(\frac{MW_{\ _pON}}{MW_{NO_{2,ON}}}\right) \quad \text{Eq. 3}$$

Where MW_{pON} refers to the average molecular weight of $_pON$ estimated from FIGAERTO-CIMS data. Assuming uniform sensitivity among detected species, MW_{pON} is similar across different experiments, within the range of 182.7-184.0 g mol^{-1}. $MW_{NO_{2,ON}}$ is the molecular weight of the nitrogen-containing moiety of ONs (*i.e.*, NO_2, 46 g mol^{-1}) measured by the HR-ToF-AMS, as discussed in detail in a recent study by Takeuchi et al. (2024). It is noted that given the limitation of FIGAERO-CIMS, which can lead to the underestimation of simple alkyl or keto nitrates (Lee et al., 2016), as well as potential differences in sensitivity among detected species, the MW_{pON} may vary.

As illustrated in Figure 5a, the time series of $_pON/OA$ stabilizes fairly quickly, similar to what we have observed previously for monoterpene systems (Takeuchi and Ng, 2019). If we utilize pseudo first-order rate equations to assess the hydrolysis lifetimes at 70% RH and 50% RH, the corresponding hydrolysis lifetimes are 18.8 ± 1.9 minutes and 29.5 ± 8.7 minutes for 70% RH and 50 % RH, respectively. Considering that a drastic change in the $_pON/OA$ ratio is not observed except for a few initial data points, the rate of $_pON$ hydrolysis may be fast enough that the decay trend of $_pON$ relative to OA is not visibly apparent. Therefore, we report the hydrolysis lifetime to be less than 30 minutes. (Takeuchi and Ng, 2019). The hydrolyzable fraction of styrene-derived ONs can be estimated from the difference in $_pON/OA$ between dry and RH

experiments once the ratio stabilizes. The hydrolyzable fraction is about 52.7-60.6%. The observed hydrolyzable ONs are $C_{16}H_{16}N_2O_8$, $C_8H_7NO_4$, and $C_8H_9NO_4$, as determined by comparing the FIGAERO-CIMS mass spectra under dry and RH 70% conditions (Figure 5b). We also observe the enhancement of non-nitrated organic species (*i.e.*, $C_8H_8O_5$) in the humid experiment, which could be formed from hydrolysis of ONs.

4. Discussion

4.1 SOA yields over a wide range of organic mass loadings

There is no prior study on SOA formation from styrene+NO_3 oxidation, but previous research has reported SOA formation from photolysis, OH-initiated photooxidation, and ozonolysis of styrene (Figure S7). Photolysis of styrene results in the lowest SOA yields, ranging from 1.8%-3.6%, in the presence of 29.4 to 202.7 μg/m^3 of ΔM_O (Tajuelo et al., 2019b). Different peroxy radical (RO_2) chemistry, controlled by the concentration of NO, influences the SOA formation during OH-initiated photooxidation of styrene. The SOA yields are observed to be 4.0-5.0% with 174.4-348.3 μg/m³ of ΔM_O in conditions where RO_2+NO chemistry dominated (Tajuelo et al., 2019b), and around 2-35 % with 2.8-430 μg/m³ of ΔM_O where RO_2+RO_2 chemistry prevailed (Yu et al., 2022b; Schueneman et al., 2024). Several previous studies have reported that the SOA yields from the ozonolysis of styrene (Ma et al., 2018; Na et al., 2006) are higher than those from OH-initiated photooxidation of styrene under RO_2+NO chemistry, but lower than those under RO_2+RO_2 chemistry. As shown in Figure S7, the SOA yield from the styrene+NO_3 oxidation is higher than in other styrene oxidation systems when ΔM_O is lower than 80 μg/m^3.

Organic vapor wall loss has been reported to impact SOA yield calculation and can lead to an underestimation of SOA yields by as much as a factor of 4 (McMurry and Grosjean, 1985; Grosjean, 1985; Matsunaga and Ziemann, 2010; Zhang et al., 2014, 2015; Yeh and Ziemann, 2015; La et al., 2016; Nah et al., 2016a; Krechmer et al., 2016; Huang et al., 2018). Therefore, to evaluate the potential effect of organic vapor wall loss on SOA yields in our study, experiments without seed particles are carried out (Exp. 9 and 10). As show in Figure S8, the SOA formation from nucleation experiments (without seed particles) is lower than condensation experiments (with seed particles). Zhang et al. (2014) determine that if organic vapor wall loss is significant in chamber experiments, the addition of more seed particles will lead to an increase in SOA yields. The differences in SOA formation between styrene+NO_3 nucleation experiments and condensation experiments suggest the possible impact of organic vapor wall loss. Although particle wall loss is accounted for, the SOA yields reported in Figure 1 and Table 1 could represent the lower limit owing to vapor wall loss, where organic vapors could have partitioned to the chamber wall rather than to the aerosols.

To account for the impact of vapor wall loss, we employ the semi-empirical equation (Eq. 1) for SOA yield to correct for vapor wall loss. The correction relies on two assumptions: (1) styrene+NO_3 oxidation

yields two major products, and (2) the partition of these major products between gas and particle phases, as well as vapor wall loss is controlled by C* of these products. The detailed procedures and the relevant equations are shown in Supplementary Information (SI). The SOA yields and the SOA yield curve after this correction is shown in Figure 1 and Table S2. The fitted molar yields (α_1 and α_2) are 0.8 and 0.1, and the fitted partitioning coefficients (K_1 and K_2) are 8.1×10^{-4} and 7.5 (corresponding to C* values of 1.2×10^{3} $\mu g/m^3$ and 1×10^{-1} $\mu g/m^3$, respectively) after vapor wall loss correction (R^2=0.991). The vapor wall loss bias factor, defined as the ratio of aerosol mass loadings after correction to those before correction, ranges from 1.3 to 3.2. The vapor wall loss bias factor is smaller for the experiments with the higher organic mass loadings, consistent with results reported by Zhang et al. (2014).

In styrene+NO_3 oxidation, two products stand out in abundance, $C_8H_9NO_4$ and $C_{16}H_{16}N_2O_8$, which constitute 92.4% of the total particle signal (Figure 3). We utilize two methods to estimate the C* of $C_8H_9NO_4$ and $C_{16}H_{16}N_2O_8$: the Estimation Program Interface Suite (EPI Suite) method and FIGAERO thermal desorption method (Takeuchi et al., 2022). The C* of $C_8H_9NO_4$ and $C_{16}H_{16}N_2O_8$, as simulated by EPI Suite, are 1.6×10^{3} $\mu g/m^3$ and 9.0×10^{-1} $\mu g/m^3$, respectively. The FIGAERO thermal desorption profiles for $C_8H_9NO_4$ and $C_{16}H_{16}N_2O_8$ are shown in Figure S9. The T_{max} of $C_8H_9NO_4$ and $C_{16}H_{16}N_2O_8$ are 24.6 and 67.8 °C, respectively, corresponding to C* values of 1.1×10^{3} and 2×10^{-1} $\mu g/m^3$. It is noted that although the FIGAERO thermal desorption profile of $C_8H_9NO_4$ shows two peaks, we use the first peak (24.6 °C) to calculate the volatility, as the second peak (around 70 °C) may result from thermal decomposition of dimers (Lopez-Hilfiker et al., 2016; Yang et al., 2021). The C* of $C_8H_9NO_4$ and $C_{16}H_{16}N_2O_8$, estimated by these two methods are similar to those obtained from the semi-empirical equation (Eq. 1). The consistency of the C* values across different methods supports the applicability of the semi-empirical equation (Eq. 1) proposed in this study for correcting vapor wall loss in SOA yield calculation.

4.2 Proposed formation mechanisms for styrene-derived organic nitrate monomers and dimers

We present the proposed formation mechanisms of major particle-phase products detected by FIGAERTO-CIMS (Figure 6). The formation mechanisms involve two distinct routes to generate the monomeric and dimeric ONs respectively. In monomeric ONs formation pathway (Pathway A): The reaction begins with the addition of a nitrooxy group (-ONO_2) onto the double bond of styrene follow by O_2 addition to form a nitrooxy peroxy radical (via R1). This addition is expected to be favored because the NO_3 radical adds to the less substituted carbon atom in the double bond. We also propose the formation mechanism with NO_3 radical adduct to the more substituted carbon atom in the double bond in Figure S10. The nitrooxy peroxy radical can further react with RO_2 or hydroperoxyl radical (HO_2) to produce the styrene hydroxy nitrate ($C_8H_9NO_4$), ketone nitrate ($C_8H_7NO_4$), and peroxy nitrate ($C_8H_9NO_5$) via reactions R2, R3, and R4, respectively. $C_8H_9NO_4$, which is the second most abundant product, has been observed in ambient environments as well. However, it has been assumed to be nitroaromatic compounds (R-NO_2, *i.e.*,

dimethoxynitrobenzene) instead of aromatic ONs (R-ONO_2) (Kong et al., 2021; Wang et al., 2021a; Salvador et al., 2021). $C_8H_9NO_5$ and $C_8H_7NO_4$ are also identified from residential wood-burning boilers and have been suggested to be nitroaromatic compounds (Salvador et al., 2021) formed from the OH-initiated photooxidation of phenolic VOCs in the presence of NO (Vione et al., 2001, 2004; Jenkin et al., 2003; Frka et al., 2016; Vidović et al., 2018). Considering the ambient concentrations of nitroaromatic compounds remain high even at night (Wang et al., 2019), our work suggests that styrene-derived ONs could account for these molecular species in ambient environments, often only attributed to nitroaromatic compounds. Furthermore, the nitrooxy peroxy radical can react with NO_3 radical to produce alkoxyl (RO) radical (via R6). The RO radical can further undergo decomposition to produce benzaldehyde, benzene hydroxy aldehyde, and NO_2 as the byproduct. NO_2 can react with nitrooxy peroxy radical as well through reaction R5 to produce styrene peroxy nitrate ($C_8H_8N_2O_7$). Peroxy nitrate remains unstable at room temperature unless there is a carbonyl group present to induce an electron-withdrawing effect, thereby stabilizing the peroxy nitrooxy group (Yu et al., 2022b). Here, the benzene ring can also stabilize the peroxy nitrooxy group through electron coupling (McMurry, 2012), thus promoting the formation of styrene peroxy nitrate. According to Lewis and Moodie (1996), NO_3 radical can react with the double bond in olefins to produce the ONs containing two nitrooxy groups. We utilize the same mechanism to elucidate the formation of $C_8H_8N_2O_6$ in our work (via R7).

The formation of nitrogen-containing dimeric products from aromatic oxidation systems has been observed in laboratory chamber studies (Molteni et al., 2018; Kumar et al., 2023; Mayorga et al., 2021). For example, Kumar et al. (2023) report that dimeric products make up 54.2% of the total particle signal in NO_3 oxidation of an aromatic hydrocarbon mixture, with the majority (42.3%) being $C_xH_yO_zN$ dimers. Nitrated diphenyl ether dimers have been observed from the NO_3 oxidation of phenolic VOCs, as reported by Mayorga et al. (2021). In our work, the predominant dimeric product is $C_{16}H_{16}N_2O_8$, which is generated from RO_2+RO_2 reaction (via R8). Additionally, $C_{16}H_{14}N_2O_8$, $C_{16}H_{17}NO_7$, $C_{15}H_{13}NO_6$, and $C_{16}H_{13}NO_6$ are also major dimeric ONs products observed in the particle phase. Benzaldehyde, ketone nitrate ($C_8H_7NO_4$), and benzene hydroxy aldehyde, can further react with NO_3 radical via reactions R9, R10, and R11 to generate radicals A1, A2, and A3, respectively. A2 and A3 can further react with each other (via R12) to terminate the radical reaction by producing $C_{16}H_{13}NO_6$. Additionally, A3 can react with RO radical from reaction R5 to form $C_{16}H_{14}N_2O_8$ (via R13), while A1 can react with nitrooxy peroxy radical to produce $C_{15}H_{13}NO_6$ (via R14). We propose the formation of $C_{16}H_{17}NO_6$ through the reaction between nitrooxy peroxy radical and styrene (via R15), followed by the RO_2 + RO_2 reaction (via R16). It is noted that in this work, we propose formation mechanisms of dimeric compounds based on molecular formulas of the detected species. Further experimental studies and density functional theory work are necessary to confirm the structures and formation of these dimeric compounds as well as detect the critical intermediates to

validate the proposed mechanism.

4.3 Hydrolysis of organic nitrates formed from styrene+NO_3 oxidation

Condensed-phase hydrolysis has been identified as a significant sink for ONs, evidenced by substantial ON uptake to aerosols and the reported short hydrolysis lifetimes (Pye et al., 2015; Fisher et al., 2016; Zare et al., 2019; Vasquez et al., 2021). Recent studies have reported experimentally constrained parameters for the hydrolysis of biogenic ONs derived from monoterpene or isoprene, through chamber or bulk solution experiments (Takeuchi and Ng, 2019; Morales et al., 2021; Hu et al., 2011; Darer et al., 2011; Jacobs et al., 2014; Rindelaub et al., 2016; Vasquez et al., 2021; Wang et al., 2021b). Studies using bulk solutions to exam hydrolysis of ONs with specific structures have demonstrated that the number of alkyl substitutions, functional groups, and carbon skeletons are three important factors controlling hydrolysis rates (Wang et al., 2021b). Therefore, the hydrolysis lifetimes of biogenic ONs can be as fast as seconds or minutes, or as stable as several days without observable hydrolysis, depending on the structures of the ONs. Unlike bulk solutions, which only involve aqueous solutions, chamber experiments can simulate the hydrolysis of ONs formed from VOC oxidations in aerosol water. In Takeuchi and Ng (2019), the ON hydrolysis lifetimes are determined to be less than 30 minutes for NO_3 oxidation and OH-initiated photooxidation of α-pinene and β-pinene systems. The hydrolysis lifetime of ONs formed from OH-initiated photooxidation of β-ocimene has been found to be pH-dependent, 51 (±13) minutes at a pH of 4 and 24 (±3) minutes at a pH of 2.5 (Morales et al., 2021).

There is limited study on the hydrolysis of anthropogenic ONs. Only one study reported the hydrolysis lifetime of ONs resulting from OH-initiated photooxidation of 1,2,4-trimethylbenzene to be 6 hours (Liu et al., 2012). The extended hydrolysis lifetime of ONs from this system can be explained by the cleavage of the benzene ring, which disrupts the delocalized π orbitals. In this study, we determine that the hydrolysis lifetime for ONs from styrene+NO_3 oxidation is less than 30 minutes. Based on our previous work with bulk solutions (Wang et al., 2021b), we propose that the benzene-related skeleton of aromatic ONs, which contains three delocalized π orbitals, can lead to rapid hydrolysis. This is because the delocalized π orbitals enhance the hyperconjugation effect and stabilize the carbocation, thereby decrease the hydrolysis lifetimes of ONs (Wang et al., 2021b). This mechanism helps explain the short hydrolysis lifetimes observed in this work.

The fraction of hydrolyzable ONs is crucial for understanding the role of hydrolysis as a loss mechanism for ONs and NO_x. Takeuchi and Ng (2019) reported that the hydrolysable fraction of ONs from the NO_3 oxidation and OH-initiated photooxidation of α-pinene and β-pinene systems range from 9-36%. However, more than 50% of the ONs resulting from the OH-initiated photooxidation of 1,2,4-trimethylbenzene are hydrolyzable (Liu et al., 2012). In our study, we observe that the fraction of hydrolyzed styrene-derived ONs ranges from 52.7% to 60.6%. Overall, while research on the fraction of

hydrolyzable ONs is still limited, these findings so far indicate that the hydrolyzable fraction of ONs resulting from the oxidation of aromatic VOCs are larger than those from biogenic VOCs. The difference can likely be explained by the fact that only ONs with specific chemical structures, particularly tertiary nitrates in biogenic VOCs oxidation systems, are susceptible to hydrolysis. In contrast, a large fraction of aromatic ONs features structures with delocalized π orbitals, which facilitate hydrolysis.

5. Atmospheric implications

To the best of our knowledge, this study is the first to demonstrate the formation of SOA and particulate ONs from styrene+NO_3 oxidation. We systematically carry out a series of chamber experiments with initial styrene concentrations ranging from 9.5 to 155.2 ppb under dry and humid conditions at room temperature. The resulting SOA yields range from 4.5% to 16.1% with the aerosol mass loadings of 1.9 to 107.4 μg/m³. It is known that the loss of organic vapors to the chamber wall can lead to underestimation of SOA yields. For instance, Zhang et al. (2014) compare the results from a statistical oxidation model and experimental observations and determine that the correction factor for SOA yields to range from 2.1 to 4.2. Here, we use a semi-empirical model that incorporates the gas-to-particle partitioning of two semi-volatile products to correct for the effect of vapor wall loss on SOA yields, the correction factor is found to range from 1.3 to 3.2, consistent with previous studies (Zhang et al., 2014). By applying the correction factor derived in this work, the corrected SOA yields range from 14.0% to 22.1% with the aerosol mass loadings of 5.9 to 147.6 μg/m³. The yields obtained in this study provide the basis to determine the contributions of styrene+NO_3 chemistry to SOA formation. Styrene has been detected at the ppb levels in ambient atmosphere and has a high emission factor from biomass burning, with typical abundance ranging from 0.06 to 45 ppb (Cho et al., 2014; Tuazon et al., 1993; Yu et al., 2019; Koss et al., 2018). These are in the range of our experiments, corresponding to the formation of up to 32.5 μg/m³ of SOA with the vapor wall loss correction. Our results serve as fundamental inputs for parameterizing SOA formation from styrene in atmospheric models.

We examine the chemical composition of SOA and propose formation mechanisms for the major monomeric and dimeric ON products detected in the particle phase. We find that dimeric products constitute around 91% of the signal, while monomeric products account for only 9%. As the fractions of monomers and dimers are relatively constant in experiments spanning a wide range of styrene concentrations, this may suggest that dimeric ONs are also important products when NO_3 reacts with typical atmospheric levels of styrene. Previous studies have suggested nitrogen-containing products measured in ambient environments are nitroaromatic compounds (R-NO_2) formed from aromatic VOCs (Kong et al., 2021; Wang et al., 2021a; Salvador et al., 2021). Our work introduces an alternative perspective, suggesting that ONs could also be nitrogen-containing products from the oxidation of aromatic VOCs in the atmosphere. Dimeric nitrogen-containing compounds from the oxidation of aromatic VOCs (*e.g.*, toluene, p-xylene, ethylbenzene, 1,3,5-trimethylbenzene, phenol, cresol, 2,6-dimethylphenol, and etc.) have been observed in chamber

experiments (Molteni et al., 2018; Kumar et al., 2023; Mayorga et al., 2021). Here, based on speciated molecular level characterization of SOA, we are able to propose the chemical structures and formation mechanisms of dimeric ON products for the first time. Besides the common RO_2+RO_2 pathway, we also suggest that other radical chain termination reactions, such as RO+R or R+R, could explain the formation of the major dimeric ONs. Further density functional theory calculations and experimental work are needed to provide additional evidence for confirming the molecular structures and identifying critical intermediates to validate our proposed mechanisms. In contrast to chamber experiments, the detection of dimeric nitrogen-containing compounds derived from aromatics is rare in field campaigns. Ye et al. (2021) observe $C_{\geqslant 19}H_yO_zN_{1\text{-}2}$ compounds in ambient aerosols in Shenzhen, China by FIGAERO-CIMS, exhibiting a ring and double-bond equivalence (RDBE) exceeding 10 and an aromaticity equivalent (Xc) surpassing 2.70 (Yassine et al., 2014; Wang et al., 2017). These compounds can be considered as aromatic ONs (Table S3). Considering the difference between controlled laboratory experiments and the complexity of ambient environments, it will be intriguing to explore why dimeric ONs derived from aromatic compounds are rarely observed in the field.

In this study, we observe that the hydrolysis lifetime of styrene-derived ONs (about 52.7 to 60.6% of total ONs) is less than 30 minutes. This finding supports our previous assumptions about the relationship between hydrolysis lifetimes and the molecular structures of ONs (Wang et al., 2021b). The unique delocalized π orbitals provided by the benzene-related skeleton of styrene ONs can stabilize the carbocation, thereby promoting hydrolysis. The hydrolysis lifetime observed for ONs generated from styrene+NO_3 oxidation can serve as experimentally constrained parameter for modeling hydrolysis of aromatic ONs in general. For example, not only styrene-derived ONs but also other aromatic ONs such as furan or methylfuran ONs (Joo et al., 2019), despite lacking benzene ring, have the potential to undergo rapid hydrolysis due to the presence of delocalized π orbitals. The hydrolysis lifetimes are crucial for regional and global chemical transport models to accurately assess the impacts of hydrolysis of aromatic ONs on the nitrogen budget and subsequent ozone formation.

Data availability.

The chamber experiment data are available online at the Index of Chamber Atmospheric Research in the United States (ICARUS, https://icarus.ucdavis.edu/).

Supporting Information

The Supporting Information is available free of charge at: https:// /acp.copernicus.org. Additional details on volatility calibration, HR-ToF-AMS and FIGAERO-CIMS mass spectra of SOA from styrene+NO_3 oxidation, representative product distribution, time series data from HR-ToF-AMS for different RH

experiments, literature review of previous styrene oxidation studies, method for correcting vapor wall loss when determining SOA yields, and other proposed mechanisms for the major particle-phase products.

Author contributions

YW and NLN designed the research. YW conducted the experiments. YW, XZ, and NLN interpreted the data and wrote the paper. YL conducted volatility calibration and YH helped with vapor wall loss correction. All the authors discussed the results and commented on the paper.

Competing interests.

The authors declare that they have no conflict of interest.

Acknowledgements

The authors would like to acknowledge financial support by the Young Scientists Fund of the National Nature Science Foundation of China (Grants 22306059), the National Science Foundation (NSF) CAREER AGS-1555034 and the National Oceanic and Atmospheric Administration (NOAA) NA18OAR4310112. This work was also supported by the Science and Technology Innovation Program of Hunan Province (Grants 2024RC3106), the Science and Technology Planning Project of Hunan Province (Grants 2023JJ40128), the Nature Science Foundation of Changsha (Grant kq2208019), the Fundamental Research Funds for the Central Universities (Grant 531118010830), and State Key Laboratory of Loess and Quaternary Geology, Institute of Earth Environment (Grant SKLLQG2235). The FIGAERO-CIMS was purchased through NSF Major Research Instrumentation (MRI) grant 1428738. The authors would also like to acknowledge Dr. Long Jia for kindly providing the raw data in his paper (Yu et al., 2022a) for Figure S7.

References:

Alfarra, M. R., Paulsen, D., Gysel, M., Garforth, A. A., Dommen, J., Prévôt, A. S. H., Worsnop, D. R., Baltensperger, U., and Coe, H.: A mass spectrometric study of secondary organic aerosols formed from the photooxidation of anthropogenic and biogenic precursors in a reaction chamber, Atmos. Chem. Phys., 6, 5279–5293, https://doi.org/10.5194/acp-6-5279-2006, 2006.

Atkinson, R. and Aschmann, S. M.: Kinetics of the reactions of acenaphthene and acenaphthylene and structurally-related aromatic compounds with OH and NO3 radicals, N2O5 and O3 at 296 ± 2 K, Int. J. Chem. Kinet., 20, 513–539, https://doi.org/10.1002/kin.550200703, 1988.

Bahreini, R., Keywood, M. D., Ng, N. L., Varutbangkul, V., Gao, S., Flagan, R. C., Seinfeld, J. H., Worsnop, D. R., and Jimenez, J. L.: Measurements of secondary organic aerosol from oxidation of cycloalkenes, terpenes, and m-xylene using an aerodyne aerosol mass spectrometer, Environ. Sci. Technol., 39,

5674–5688, https://doi.org/10.1021/es048061a, 2005.

Boyd, C. M., Sanchez, J., Xu, L., Eugene, A. J., Nah, T., Tuet, W. Y., Guzman, M. I., and Ng, N. L.: Secondary organic aerosol formation from the β-pinene+NO3 system: Effect of humidity and peroxy radical fate, Atmos. Chem. Phys., 15, 7497–7522, https://doi.org/10.5194/acp-15-7497-2015, 2015.

Boyd, C. M., Nah, T., Xu, L., Berkemeier, T., and Ng, N. L.: Secondary Organic Aerosol (SOA) from Nitrate Radical Oxidation of Monoterpenes: Effects of Temperature, Dilution, and Humidity on Aerosol Formation, Mixing, and Evaporation, Environ. Sci. Technol., 51, 7831–7841, https://doi.org/10.1021/acs.est.7b01460, 2017.

Cabrera-Perez, D., Taraborrelli, D., Sander, R., and Pozzer, A.: Global atmospheric budget of simple monocyclic aromatic compounds, Atmos. Chem. Phys., 16, 6931–6947, https://doi.org/10.5194/acp-16-6931-2016, 2016.

Calvert, J. G., Atkinson, R., Becker, K. H., Kamens, R. M., Seinfeld, J. H., Wallington, T. H., and Yarwood, G.: The Mechanisms of Atmospheric Oxidation of the Aromatic Hydrocarbons, Oxford University Press, 2002.

Canagaratna, M. R., Jimenez, J. L., Kroll, J. H., Chen, Q., Kessler, S. H., Massoli, P., Hildebrandt Ruiz, L., Fortner, E., Williams, L. R., Wilson, K. R., Surratt, J. D., Donahue, N. M., Jayne, J. T., and Worsnop, D. R.: Elemental ratio measurements of organic compounds using aerosol mass spectrometry: Characterization, improved calibration, and implications, Atmos. Chem. Phys., 15, 253–272, https://doi.org/10.5194/acp-15-253-2015, 2015.

Chen, T., Chu, B., Ma, Q., Zhang, P., Liu, J., and He, H.: Effect of relative humidity on SOA formation from aromatic hydrocarbons: Implications from the evolution of gas- and particle-phase species, Sci. Total Environ., 773, 145015, https://doi.org/10.1016/j.scitotenv.2021.145015, 2021.

Chen, Y., Takeuchi, M., Nah, T., Xu, L., Canagaratna, M. R., Stark, H., Baumann, K., Canonaco, F., Prevot, A. S. H., Gregory Huey, L., Weber, R. J., and Ng, N. L.: Chemical characterization of secondary organic aerosol at a rural site in the southeastern US: Insights from simultaneous high-resolution time-of-flight aerosol mass spectrometer (HR-ToF-AMS) and FIGAERO chemical ionization mass spectrometer (CIMS) measur, Atmos. Chem. Phys., 20, 8421–8440, https://doi.org/10.5194/acp-20-8421-2020, 2020.

Cho, J., Roueintan, M., and Li, Z.: Kinetic and dynamic investigations of oh reaction with styrene, J. Phys. Chem. A, 118, 9460–9470, https://doi.org/10.1021/jp501380j, 2014.

Darer, A. I., Cole-Filipiak, N. C., O'Connor, A. E., and Elrod, M. J.: Formation and stability of atmospherically relevant isoprene-derived organosulfates and organonitrates, Environ. Sci. Technol., 45, 1895–1902, https://doi.org/10.1021/es103797z, 2011.

Day, D. A., Campuzano-jost, P., Nault, B. A., Palm, B. B., Hu, W., Martin, S. T., and Jimenez, J. L.: A

systematic re-evaluation of methods for quantification of bulk particle-phase organic nitrates using real-time aerosol mass spectrometry, Atmos. Meas. Tech., 15, 459–483, 2022.

DeCarlo, P. F., Kimmel, J. R., Trimborn, A., Northway, M. J., Jayne, J. T., Aiken, A. C., Gonin, M., Fuhrer, K., Horvath, T., Docherty, K. S., Worsnop, D. R., and Jimenez, J. L.: Field-deployable, high-resolution, time-of-flight aerosol mass spectrometer, Anal. Chem., 78, 8281–8289, https://doi.org/10.1021/ac061249n, 2006.

Decker, Z. C. J., Robinson, M. A., Barsanti, K. C., Bourgeois, I., Coggon, M. M., Digangi, J. P., Diskin, G. S., Flocke, F. M., Franchin, A., Fredrickson, C. D., Gkatzelis, G. I., Hall, S. R., Halliday, H., Holmes, C. D., Huey, L. G., Lee, Y. R., Lindaas, J., Middlebrook, A. M., Montzka, D. D., Moore, R., Neuman, J. A., Nowak, J. B., Palm, B. B., Peischl, J., Piel, F., Rickly, P. S., Rollins, A. W., Ryerson, T. B., Schwantes, R. H., Sekimoto, K., Thornhill, L., Thornton, J. A., Tyndall, G. S., Ullmann, K., Van Rooy, P., Veres, P. R., Warneke, C., Washenfelder, R. A., Weinheimer, A. J., Wiggins, E., Winstead, E., Wisthaler, A., Womack, C., and Brown, S. S.: Nighttime and daytime dark oxidation chemistry in wildfire plumes: An observation and model analysis of FIREX-AQ aircraft data, Atmos. Chem. Phys., 21, 16293–16317, https://doi.org/10.5194/acp-21-16293-2021, 2021.

Farmer, D. K., Matsunaga, A., Docherty, K. S., Surratt, J. D., Seinfeld, J. H., Ziemann, P. J., and Jimenez, J. L.: Response of an aerosol mass spectrometer to organonitrates and organosulfates and implications for atmospheric chemistry, Proc. Natl. Acad. Sci. U. S. A., 107, 6670–6675, https://doi.org/10.1073/pnas.0912340107, 2010.

Fisher, J. A., Jacob, D. J., Travis, K. R., Kim, P. S., Marais, E. A., Miller, C. C., Yu, K., Zhu, L., Yantosca, R. M., Sulprizio, M. P., Mao, J., Wennberg, P. O., Crounse, J. D., Teng, A. P., Nguyen, T. B., Clair, J. M. S., Cohen, R. C., Romer, P., Nault, B. A., Wooldridge, P. J., Jimenez, J. L., Campuzano-Jost, P., Day, D. A., Hu, W., Shepson, P. B., Xiong, F., Blake, D. R., Goldstein, A. H., Misztal, P. K., Hanisco, T. F., Wolfe, G. M., Ryerson, T. B., Wisthaler, A., and Mikoviny, T.: Organic nitrate chemistry and its implications for nitrogen budgets in an isoprene- and monoterpene-rich atmosphere: Constraints from aircraft (SEAC4RS) and ground-based (SOAS) observations in the Southeast US, 5969–5991 pp., https://doi.org/10.5194/acp-16-5969-2016, 2016.

Frka, S., Šala, M., Kroflič, A., Huš, M., Čusak, A., and Grgić, I.: Quantum Chemical Calculations Resolved Identification of Methylnitrocatechols in Atmospheric Aerosols, Environ. Sci. Technol., 50, 5526–5535, https://doi.org/10.1021/acs.est.6b00823, 2016.

Grosjean, D.: Wall Loss of Gaseous Pollutants in Outdoor Teflon Chambers, Environ. Sci. Technol., 19, 1059–1065, https://doi.org/10.1021/es00141a006, 1985.

Helal, S. F. and Elshafy, W. S.: Health hazards among workers in plastic industry, Toxicol. Ind. Health, 29, 812–819, https://doi.org/10.1177/0748233712442728, 2012.

Henry, K. M. and Donahue, N. M.: Photochemical aging of α-pinene secondary organic aerosol: Effects of OH radical sources and photolysis, J. Phys. Chem. A, 116, 5932–5940, https://doi.org/10.1021/jp210288s, 2012.

Hu, K. S., Darer, A. I., and Elrod, M. J.: Thermodynamics and kinetics of the hydrolysis of atmospherically relevant organonitrates and organosulfates, Atmos. Chem. Phys., 11, 8307–8320, https://doi.org/10.5194/acp-11-8307-2011, 2011.

Huang, Y., Zhao, R., Charan, S. M., Kenseth, C. M., Zhang, X., and Seinfeld, J. H.: Unified Theory of Vapor-Wall Mass Transport in Teflon-Walled Environmental Chambers, Environ. Sci. Technol., 52, 2134–2142, https://doi.org/10.1021/acs.est.7b05575, 2018.

Jacobs, M. I., Burke, W. J., and Elrod, M. J.: Kinetics of the reactions of isoprene-derived hydroxynitrates: Gas phase epoxide formation and solution phase hydrolysis, Atmos. Chem. Phys., 14, 8933–8946, https://doi.org/10.5194/acp-14-8933-2014, 2014.

Jenkin, M. E., Saunders, S. M., Wagner, V., and Pilling, M. J.: Protocol for the development of the Master Chemical Mechanism, MCM v3 (Part B): Tropospheric degradation of aromatic volatile organic compounds, Atmos. Chem. Phys., 3, 181–193, https://doi.org/10.5194/acp-3-181-2003, 2003.

Jiang, H., Cai, J., Feng, X., Chen, Y., Wang, L., Jiang, B., Liao, Y., Li, J., Zhang, G., Mu, Y., and Chen, J.: Aqueous-Phase Reactions of Anthropogenic Emissions Lead to the High Chemodiversity of Atmospheric Nitrogen-Containing Compounds during the Haze Event, Environ. Sci. Technol., 57, 16500–16511, https://doi.org/10.1021/acs.est.3c06648, 2023.

Joo, T., Rivera-Rios, J. C., Takeuchi, M., Alvarado, M. J., and Ng, N. L.: Secondary Organic Aerosol Formation from Reaction of 3-Methylfuran with Nitrate Radicals, ACS Earth Sp. Chem., 3, 922–934, https://doi.org/10.1021/acsearthspacechem.9b00068, 2019.

Kinney, P. D., Pui, D. Y. H., Mulholland, G. W., and Bryner, N. P.: Use of the electrostatic classification method to size 0.1 micrometer SRM particles - A feasibility study, J. Res. Natl. Inst. Stand. Technol., 96, 147, https://doi.org/10.6028/jres.096.006, 1991.

Knighton, W. B., Herndon, S. C., Wood, E. C., Fortner, E. C., Onasch, T. B., Wormhoudt, J., Kolb, C. E., Lee, B. H., Zavala, M., Molina, L., and Jones, M.: Detecting fugitive emissions of 1,3-butadiene and styrene from a petrochemical facility: An application of a mobile laboratory and a modified proton transfer reaction mass spectrometer, Ind. Eng. Chem. Res., 51, 12706–12711, https://doi.org/10.1021/ie202794j, 2012.

Kong, X., Salvador, C. M., Carlsson, S., Pathak, R., Davidsson, K. O., Le Breton, M., Gaita, S. M., Mitra, K., Hallquist, Å. M., Hallquist, M., and Pettersson, J. B. C.: Molecular characterization and optical properties of primary emissions from a residential wood burning boiler, Sci. Total Environ., 754, 142143, https://doi.org/10.1016/j.scitotenv.2020.142143, 2021.

Koss, A. R., Sekimoto, K., Gilman, J. B., Selimovic, V., Coggon, M. M., Zarzana, K. J., Yuan, B., Lerner, B. M., Brown, S. S., Jimenez, J. L., Krechmer, J., Roberts, J. M., Warneke, C., Yokelson, R. J., and De Gouw, J.: Non-methane organic gas emissions from biomass burning: Identification, quantification, and emission factors from PTR-ToF during the FIREX 2016 laboratory experiment, Atmos. Chem. Phys., 18, 3299–3319, https://doi.org/10.5194/acp-18-3299-2018, 2018.

Krechmer, J. E., Pagonis, D., Ziemann, P. J., and Jimenez, J. L.: Quantification of Gas-Wall Partitioning in Teflon Environmental Chambers Using Rapid Bursts of Low-Volatility Oxidized Species Generated in Situ, Environ. Sci. Technol., 50, 5757–5765, https://doi.org/10.1021/acs.est.6b00606, 2016.

Kumar, V., Slowik, J. G., Baltensperger, U., Prevot, A. S. H., and Bell, D. M.: Time-Resolved Molecular Characterization of Secondary Organic Aerosol Formed from OH and NO3 Radical Initiated Oxidation of a Mixture of Aromatic Precursors, Environ. Sci. Technol., 57, 11572–11582, https://doi.org/10.1021/acs.est.3c00225, 2023.

La, Y. S., Camredon, M., Ziemann, P. J., Valorso, R., Matsunaga, A., Lannuque, V., Lee-Taylor, J., Hodzic, A., Madronich, S., and Aumont, B.: Impact of chamber wall loss of gaseous organic compounds on secondary organic aerosol formation: Explicit modeling of SOA formation from alkane and alkene oxidation, Atmos. Chem. Phys., 16, 1417–1431, https://doi.org/10.5194/acp-16-1417-2016, 2016.

Lee, B. H., Mohr, C., Lopez-Hilfiker, F. D., Lutz, A., Hallquist, M., Lee, L., Romer, P., Cohen, R. C., Iyer, S., Kurtén, T., Hu, W., Day, D. A., Campuzano-Jost, P., Jimenez, J. L., Xu, L., Ng, N. L., Guo, H., Weber, R. J., Wild, R. J., Brown, S. S., Koss, A., Gouw, J. de, Olson, K., Goldstein, A. H., Seco, R., Kim, S., McAvey, K., Shepson, P. B., Starn, T., Baumann, K., Edgerton, E. S., Liu, J., Shilling, J. E., Miller, D. O., Brune, W., Schobesberger, S., D'Ambro, E. L., and Thornton, J. A.: Highly functionalized organic nitrates in the southeast United States: Contribution to secondary organic aerosol and reactive nitrogen budgets, Proc. Natl. Acad. Sci., 113, 1516–1521, https://doi.org/10.1073/PNAS.1508108113, 2016.

Lewis, R. J. and Moodie, R. B.: Nitration of styrenes by dinitrogen pentoxide in dichloromethane, J. Chem. Soc. Perkin Trans. 2, 1315–1320, 1996.

Lin, C., Huang, R. J., Duan, J., Zhong, H., and Xu, W.: Primary and Secondary Organic Nitrate in Northwest China: A Case Study, Environ. Sci. Technol. Lett., 8, 947–953, https://doi.org/10.1021/acs.estlett.1c00692, 2021.

Liu, S., Shilling, J. E., Song, C., Hiranuma, N., Zaveri, R. A., and Russell, L. M.: Hydrolysis of organonitrate functional groups in aerosol particles, Aerosol Sci. Technol., 46, 1359–1369, https://doi.org/10.1080/02786826.2012.716175, 2012.

Liu, S., Liu, X., Wang, Y., Zhang, S., Wu, C., Du, W., and Wang, G.: Effect of NOx and RH on the secondary organic aerosol formation from toluene photooxidation, J. Environ. Sci. (China), 114, 1–9,

https://doi.org/10.1016/j.jes.2021.06.017, 2022.

Lopez-Hilfiker, F. D., Mohr, C., Ehn, M., Rubach, F., Kleist, E., Wildt, J., Mentel, T. F., Lutz, A., Hallquist, M., Worsnop, D., and Thornton, J. A.: A novel method for online analysis of gas and particle composition: Description and evaluation of a filter inlet for gases and AEROsols (FIGAERO), Atmos. Meas. Tech., 7, 983–1001, https://doi.org/10.5194/amt-7-983-2014, 2014.

Lopez-Hilfiker, F. D., Mohr, C., D'Ambro, E. L., Lutz, A., Riedel, T. P., Gaston, C. J., Iyer, S., Zhang, Z., Gold, A., Surratt, J. D., Lee, B. H., Kurten, T., Hu, W. W., Jimenez, J., Hallquist, M., and Thornton, J. A.: Molecular Composition and Volatility of Organic Aerosol in the Southeastern U.S.: Implications for IEPOX Derived SOA, Environ. Sci. Technol., 50, 2200–2209, https://doi.org/10.1021/acs.est.5b04769, 2016.

Lu, B., Meng, X., Dong, S., Zhang, Z., Liu, C., Jiang, J., Herrmann, H., and Li, X.: High-resolution mapping of regional VOCs using the enhanced space-time extreme gradient boosting machine (XGBoost) in Shanghai, Sci. Total Environ., 905, 167054, https://doi.org/10.1016/j.scitotenv.2023.167054, 2023a.

Lu, Y., Ma, Y., Huang, D. D., Lou, S., Jing, S., Gao, Y., Wang, H., Zhang, Y., Chen, H., Chang, Y., Yan, N., Chen, J., George, C., Riva, M., and Huang, C.: Unambiguous identification of N-containing oxygenated organic molecules using a chemical-ionization Orbitrap (CI-Orbitrap) in an eastern Chinese megacity, Atmos. Chem. Phys., 23, 3233–3245, https://doi.org/10.5194/acp-23-3233-2023, 2023b.

Ma, Q., Lin, X., Yang, C., Long, B., Gai, Y., and Zhang, W.: The influences of ammonia on aerosol formation in the ozonolysis of styrene: Roles of criegee intermediate reactions, R. Soc. Open Sci., 5, 172171–172183, https://doi.org/10.1098/rsos.172171, 2018.

Matsunaga, A. and Ziemann, P. J.: Gas-wall partitioning of organic compounds in a teflon film chamber and potential effects on reaction product and aerosol yield measurements, Aerosol Sci. Technol., 44, 881–892, https://doi.org/10.1080/02786826.2010.501044, 2010.

Mayorga, R. J., Zhao, Z., and Zhang, H.: Formation of secondary organic aerosol from nitrate radical oxidation of phenolic VOCs: Implications for nitration mechanisms and brown carbon formation, Atmos. Environ., 244, 117910, https://doi.org/10.1016/j.atmosenv.2020.117910, 2021.

McLafferty, F. W. and Turecek, F.: Interpretation Of Mass Spectra, University Science Books, 1993.

McMurry, J.: Organic Chemistry, Brooks/Cole Cengage Learning, 2012.

McMurry, P. H. and Grosjean, D.: Gas and Aerosol Wall Losses in Teflon Film Smog Chambers, Environ. Sci. Technol., 19, 1176–1182, https://doi.org/10.1021/es00142a006, 1985.

Molteni, U., Bianchi, F., Klein, F., El Haddad, I., Frege, C., Rossi, M. J., Dommen, J., and Baltensperger, U.: Formation of highly oxygenated organic molecules from aromatic compounds, Atmos. Chem. Phys., 18, 1909–1921, https://doi.org/10.5194/acp-18-1909-2018, 2018.

Morales, A. C., Jayarathne, T., Slade, J. H., Laskin, A., and Shepson, P. B.: The production and hydrolysis of organic nitrates from OH radical oxidation of β-ocimene, Atmos. Chem. Phys., 21, 129–145, https://doi.org/10.5194/acp-21-129-2021, 2021.

Na, K., Song, C., and Cocker, D. R.: Formation of secondary organic aerosol from the reaction of styrene with ozone in the presence and absence of ammonia and water, Atmos. Environ., 40, 1889–1900, https://doi.org/10.1016/j.atmosenv.2005.10.063, 2006.

Nah, T., Mcvay, R. C., Zhang, X., Boyd, C. M., Seinfeld, J. H., and Ng, N. L.: Influence of seed aerosol surface area and oxidation rate on vapor wall deposition and SOA mass yields : a case study with α - pinene ozonolysis, Atmos. Chem. Phys., 16, 9361–9379, https://doi.org/10.5194/acp-16-9361-2016, 2016a.

Nah, T., Sanchez, J., Boyd, C. M., and Ng, N. L.: Photochemical Aging of α-pinene and β-pinene Secondary Organic Aerosol formed from Nitrate Radical Oxidation, Environ. Sci. Technol., 50, 222–231, https://doi.org/10.1021/acs.est.5b04594, 2016b.

Nah, T., McVay, R. C., Pierce, J. R., Seinfeld, J. H., and Ng, N. L.: Constraining uncertainties in particle-wall deposition correction during SOA formation in chamber experiments, Atmos. Chem. Phys., 17, 2297–2310, https://doi.org/10.5194/acp-17-2297-2017, 2017.

Ng, L. N., Brown, S. S., Archibald, A. T., Atlas, E., Cohen, R. C., Crowley, J. N., Day, D. A., Donahue, N. M., Fry, J. L., Fuchs, H., Griffin, R. J., Guzman, M. I., Herrmann, H., Hodzic, A., Iinuma, Y., Kiendler-Scharr, A., Lee, B. H., Luecken, D. J., Mao, J., McLaren, R., Mutzel, A., Osthoff, H. D., Ouyang, B., Picquet-Varrault, B., Platt, U., Pye, H. O. T., Rudich, Y., Schwantes, R. H., Shiraiwa, M., Stutz, J., Thornton, J. A., Tilgner, A., Williams, B. J., and Zaveri, R. A.: Nitrate radicals and biogenic volatile organic compounds: Oxidation, mechanisms, and organic aerosol, Atmos. Chem. Phys., 17, 2103–2162, https://doi.org/10.5194/acp-17-2103-2017, 2017.

Ng, N. L., Kwan, A. J., Surratt, J. D., Chan, A. W. H., Chhabra, P. S., Sorooshian, A., Pye, H. O. T., Crounse, J. D., Wennberg, P. O., Flagan, R. C., and Seinfeld, J. H.: Secondary organic aerosol (SOA) formation from reaction of isoprene with nitrate radicals (NO3), Atmos. Chem. Phys., 8, 4117–4140, https://doi.org/10.5194/acp-8-4117-2008, 2008.

Odum, J. R., Hoffmann, T., Bowman, F., Collins, D., Flagan, R. C., and Seinfeld, J. H.: Gas/particle partitioning and secondary organic aerosol yields, Environ. Sci. Technol., 30, 2580–2585, https://doi.org/10.1021/es950943+, 1996.

Odum, J. R., Jungkamp, T. P. W., Griffin, R. J., Flagan, R. C., and Seinfeld, J. H.: The Atmospheric Aerosol-Forming Potential of Whole Gasoline Vapor, Science (80-.)., 276, 96–99, https://doi.org/10.1126/science.276.5309.96, 1997.

Okada, Y., Nakagoshi, A., Tsurukawa, M., Matsumura, C., Eiho, J., and Nakano, T.: Environmental risk

assessment and concentration trend of atmospheric volatile organic compounds in Hyogo Prefecture, Japan, Environ. Sci. Pollut. Res., 19, 201–213, https://doi.org/10.1007/s11356-011-0550-0, 2012.

Orel, A. E., Peterson, T. W., and Seinfeld, J. H.: Nitrate Formation in Atmospheric Aerosols., Environ. Sci. Technol., 18, 410–411, https://doi.org/10.1021/es60142a016, 1978.

Le Person, A., Eyglunent, G., Daële, V., Mellouki, A., and Mu, Y.: The near UV absorption cross-sections and the rate coefficients for the ozonolysis of a series of styrene-like compounds, J. Photochem. Photobiol. A Chem., 195, 54–63, https://doi.org/10.1016/j.jphotochem.2007.09.006, 2008.

Pye, H. O. T., Luecken, D. J., Xu, L., Boyd, C. M., Ng, N. L., Baker, K. R., Ayres, B. R., Bash, J. O., Baumann, K., Carter, W. P. L., Edgerton, E., Fry, J. L., Hutzell, W. T., Schwede, D. B., and Shepson, P. B.: Modeling the Current and Future Roles of Particulate Organic Nitrates in the Southeastern United States, Environ. Sci. Technol., 49, 14195–14203, https://doi.org/10.1021/acs.est.5b03738, 2015.

Rindelaub, J. D., Borca, C. H., Hostetler, M. A., Slade, J. H., Lipton, M. A., Slipchenko, L. V., and Shepson, P. B.: The acid-catalyzed hydrolysis of an α-pinene-derived organic nitrate: Kinetics, products, reaction mechanisms, and atmospheric impact, Atmos. Chem. Phys., 16, 15425–15432, https://doi.org/10.5194/acp-16-15425-2016, 2016.

Salvador, C. M. G., Tang, R., Priestley, M., Li, L., Tsiligiannis, E., Le Breton, M., Zhu, W., Zeng, L., Wang, H., Yu, Y., Hu, M., Guo, S., and Hallquist, M.: Ambient nitro-aromatic compounds-biomass burning versus secondary formation in rural China, Atmos. Chem. Phys., 21, 1389–1406, https://doi.org/10.5194/acp-21-1389-2021, 2021.

Schueneman, M. K., Day, D. A., Peng, Z., Pagonis, D., Jenks, O. J., de Gouw, J. A., and Jimenez, J. L.: Secondary Organic Aerosol Formation from the OH Oxidation of Phenol, Catechol, Styrene, Furfural, and Methyl Furfural, ACS Earth Sp. Chem., 8, 1179–1192, https://doi.org/10.1021/acsearthspacechem.3c00361, 2024.

Stark, H., Yatavelli, R. L. N., Thompson, S. L., Kang, H., Krechmer, J. E., Kimmel, J. R., Palm, B. B., Hu, W., Hayes, P. L., Day, D. A., Campuzano-Jost, P., Canagaratna, M. R., Jayne, J. T., Worsnop, D. R., and Jimenez, J. L.: Impact of Thermal Decomposition on Thermal Desorption Instruments: Advantage of Thermogram Analysis for Quantifying Volatility Distributions of Organic Species, Environ. Sci. Technol., 51, 8491–8500, https://doi.org/10.1021/acs.est.7b00160, 2017.

Sun, J., Wu, F., Hu, B., Tang, G., Zhang, J., and Wang, Y.: VOC characteristics, emissions and contributions to SOA formation during hazy episodes, Atmos. Environ., 141, 560–570, https://doi.org/10.1016/j.atmosenv.2016.06.060, 2016.

Tajuelo, M., Bravo, I., Rodríguez, A., Aranda, A., Díaz-de-Mera, Y., and Rodríguez, D.: Atmospheric sink of styrene, A-methylstyrene, trans-B-methylstyrene and indene: Rate constants and mechanisms of Cl

atom-initiated degradation, Atmos. Environ., 200, 78–89, https://doi.org/10.1016/j.atmosenv.2018.11.059, 2019a.

Tajuelo, M., Rodríguez, D., Baeza-Romero, M. T., Díaz-de-Mera, Y., Aranda, A., and Rodríguez, A.: Secondary organic aerosol formation from styrene photolysis and photooxidation with hydroxyl radicals, Chemosphere, 231, 276–286, https://doi.org/10.1016/j.chemosphere.2019.05.136, 2019b.

Takeuchi, M. and Ng, N. L.: Chemical composition and hydrolysis of organic nitrate aerosol formed from hydroxyl and nitrate rlanadical oxidation of α-pinene and β-pinene, Atmos. Chem. Phys., 19, 12749–12766, https://doi.org/10.5194/acp-19-12749-2019, 2019.

Takeuchi, M., Berkemeier, T., Eris, G., and Ng, N. L.: Non-linear effects of secondary organic aerosol formation and properties in multi-precursor systems, Nat. Commun., 13, 1–13, https://doi.org/10.1038/s41467-022-35546-1, 2022.

Takeuchi, M., Wang, Y., Nault, B. A., Chen, Y., Canagaratna, M. R., and Ng, N. L.: Evaluating the response of the Aerodyne aerosol mass spectrometer to monoterpene- and isoprene-derived organic nitrate standards, Aerosol Sci. Technol., 0, 1–18, https://doi.org/10.1080/02786826.2024.2389183, 2024.

Tasoglou, A. and Pandis, S. N.: Formation and chemical aging of secondary organic aerosol during the β-caryophyllene oxidation, Atmos. Chem. Phys., 15, 6035–6046, https://doi.org/10.5194/acp-15-6035-2015, 2015.

Thornton, J. A., Mohr, C., Schobesberger, S., D'Ambro, E. L., Lee, B. H., and Lopez-Hilfiker, F. D.: Evaluating Organic Aerosol Sources and Evolution with a Combined Molecular Composition and Volatility Framework Using the Filter Inlet for Gases and Aerosols (FIGAERO), Acc. Chem. Res., 53, 1415–1426, https://doi.org/10.1021/acs.accounts.0c00259, 2020.

Tuazon, E. C., Arey, J., Atkinson, R., and Aschmann, S. M.: Gas-Phase Reactions of 2-Vinylpyridine and Styrene with OH and NO3 Radicals and O3, Environ. Sci. Technol., 27, 1832–1841, https://doi.org/10.1021/es00046a011, 1993.

Vasquez, K. T., Crounse, J. D., Schulze, B. C., Bates, K. H., Teng, A. P., Xu, L., Allen, H. M., and Wennberg, P. O.: Rapid hydrolysis of tertiary isoprene nitrate efficiently removes NOx from the atmosphere, Proc. Natl. Acad. Sci. U. S. A., 117, 33011–33016, https://doi.org/10.1073/PNAS.2017442117, 2021.

Vidović, K., Lašič Jurković, D., Šala, M., Kroflič, A., and Grgić, I.: Nighttime Aqueous-Phase Formation of Nitrocatechols in the Atmospheric Condensed Phase, Environ. Sci. Technol., 52, 9722–9730, https://doi.org/10.1021/acs.est.8b01161, 2018.

Vione, D., Maurino, V., Minero, C., and Pelizzetti, E.: Phenol photonitration upon UV irradiation of nitrite in aqueous solution I: Effects of oxygen and 2-propanol, Chemosphere, 45, 893–902, https://doi.org/10.1016/S0045-6535(01)00035-2, 2001.

784 Vione, D., Maurino, V., Minero, C., Lucchiari, M., and Pelizzetti, E.: Nitration and hydroxylation of
785 benzene in the presence of nitrite/nitrous acid in aqueous solution, Chemosphere, 56, 1049–1059,
786 https://doi.org/10.1016/j.chemosphere.2004.05.027, 2004.
787 Wang, H., Ji, Y., Gao, Y., Li, G., and An, T.: Theoretical model on the formation possibility of secondary
788 organic aerosol from OH initialed oxidation reaction of styrene in the presence of O2/NO, Atmos.
789 Environ., 101, 1–9, https://doi.org/10.1016/j.atmosenv.2014.10.042, 2015.
790 Wang, W., Zhang, Y., Jiang, B., Chen, Y., Song, Y., Tang, Y., Dong, C., and Cai, Z.: Molecular
791 characterization of organic aerosols in Taiyuan, China: Seasonal variation and source identification,
792 Sci. Total Environ., 800, 149419, https://doi.org/10.1016/j.scitotenv.2021.149419, 2021a.
793 Wang, X., Hayeck, N., Brüggemann, M., Yao, L., Chen, H., Zhang, C., Emmelin, C., Chen, J., George, C.,
794 and Wang, L.: Chemical Characteristics of Organic Aerosols in Shanghai: A Study by Ultrahigh-
795 Performance Liquid Chromatography Coupled With Orbitrap Mass Spectrometry, J. Geophys. Res.
796 Atmos., 122, 11,703-11,722, https://doi.org/10.1002/2017JD026930, 2017.
797 Wang, Y., Hu, M., Wang, Y., Zheng, J., Shang, D., Yang, Y., Liu, Y., Li, X., Tang, R., Zhu, W., Du, Z.,
798 Wu, Y., Guo, S., Wu, Z., Lou, S., Hallquist, M., and Yu, J. Z.: The formation of nitro-aromatic
799 compounds under high NOx and anthropogenic VOC conditions in urban Beijing, China, Atmos.
800 Chem. Phys., 19, 7649–7665, https://doi.org/10.5194/acp-19-7649-2019, 2019.
801 Wang, Y., Piletic, I. R., Takeuchi, M., Xu, T., France, S., and Ng, N. L.: Synthesis and Hydrolysis of
802 Atmospherically Relevant Monoterpene-Derived Organic Nitrates, Environ. Sci. Technol., 55, 14595–
803 14606, https://doi.org/10.1021/acs.est.1c05310, 2021b.
804 Wu, S., Tang, G., Wang, Y., Yang, Y., Yao, D., Zhao, W., Gao, W., Sun, J., and Wang, Y.: Vertically
805 decreased VOC concentration and reactivity in the planetary boundary layer in winter over the North
806 China Plain, Atmos. Res., 240, 104930, https://doi.org/10.1016/j.atmosres.2020.104930, 2020.
807 Yang, L. H., Takeuchi, M., Chen, Y., and Ng, N. L.: Characterization of thermal decomposition of
808 oxygenated organic compounds in FIGAERO-CIMS, Aerosol Sci. Technol., 55, 1321–1342,
809 https://doi.org/10.1080/02786826.2021.1945529, 2021.
810 Yang, X., Luo, F., Li, J., Chen, D., Ye, E., Lin, W., and Jin, J.: Alkyl and aromatic nitrates in atmospheric
811 particles determined by gas chromatography tandem mass spectrometry, J. Am. Soc. Mass Spectrom.,
812 30, 2762–2770, https://doi.org/10.1007/s13361-019-02347-8, 2019.
813 Yang, Y., Wang, Y., Zhou, P., Yao, D., Ji, D., Sun, J., Wang, Y., Zhao, S., Huang, W., Yang, S., Chen, D.,
814 Gao, W., Liu, Z., Hu, B., Zhang, R., Zeng, L., Ge, M., Petäjä, T., Kerminen, V. M., Kulmala, M., and
815 Wang, Y.: Atmospheric reactivity and oxidation capacity during summer at a suburban site between
816 Beijing and Tianjin, Atmos. Chem. Phys., 20, 8181–8200, https://doi.org/10.5194/acp-20-8181-2020,
817 2020.

Yassine, M. M., Harir, M., Dabek-Zlotorzynska, E., and Schmitt-Kopplin, P.: Structural characterization of organic aerosol using Fourier transform ion cyclotron resonance mass spectrometry: aromaticity equivalent approach, Rapid Commun. Mass Spectrom., 28, 2445–2454, https://doi.org/10.1002/rcm.7038, 2014.

Ye, C., Yuan, B., Lin, Y., Wang, Z., Hu, W., Li, T., Chen, W., Wu, C., Wang, C., Huang, S., Qi, J., Wang, B., Wang, C., Song, W., Wang, X., Zheng, E., Krechmer, J. E., Ye, P., Zhang, Z., Wang, X., Worsnop, D. R., and Shao, M.: Chemical characterization of oxygenated organic compounds in the gas phase and particle phase using iodide CIMS with FIGAERO in urban air, Atmos. Chem. Phys., 21, 8455–8478, https://doi.org/10.5194/acp-21-8455-2021, 2021.

Yeh, G. K. and Ziemann, P. J.: Gas-wall partitioning of oxygenated organic compounds: Measurements, structure-activity relationships, and correlation with gas chromatographic retention factor, Aerosol Sci. Technol., 49, 727–738, https://doi.org/10.1080/02786826.2015.1068427, 2015.

Ylisirniö, A., Barreira, L. M. F., Pullinen, I., Buchholz, A., Jayne, J., Krechmer, J. E., Worsnop, D. R., Virtanen, A., and Schobesberger, S.: On the calibration of FIGAERO-ToF-CIMS: Importance and impact of calibrant delivery for the particle-phase calibration, Atmos. Meas. Tech., 14, 355–367, https://doi.org/10.5194/amt-14-355-2021, 2021.

Yu, K., Zhu, Q., Du, K., and Huang, X.: Characterization of nighttime formation of particulate organic nitrates based on high-resolution aerosol mass spectrometry in an urban atmosphere in China, Atmos. Chem. Phys., 19, 5235–5249, 2019.

Yu, L., Smith, J., Laskin, A., Anastasio, C., Laskin, J., and Zhang, Q.: Chemical characterization of SOA formed from aqueous-phase reactions of phenols with the triplet excited state of carbonyl and hydroxyl radical, Atmos. Chem. Phys., 14, 13801–13816, https://doi.org/10.5194/acp-14-13801-2014, 2014.

Yu, L., Smith, J., Laskin, A., M George, K., Anastasio, C., Laskin, J., M Dillner, A., and Zhang, Q.: Molecular transformations of phenolic SOA during photochemical aging in the aqueous phase: Competition among oligomerization, functionalization, and fragmentation, Atmos. Chem. Phys., 16, 4511–4527, https://doi.org/10.5194/acp-16-4511-2016, 2016.

Yu, S., Jia, L., Xu, Y., and Pan, Y.: Formation of extremely low-volatility organic compounds from styrene ozonolysis: Implication for nucleation, Chemosphere, 305, 135459, https://doi.org/10.1016/j.chemosphere.2022.135459, 2022a.

Yu, S. S., Jia, L., Xu, Y. F., and Pan, Y. P.: Molecular composition of secondary organic aerosol from styrene under different NOx and humidity conditions, Atmos. Res., 266, 105950, https://doi.org/10.1016/j.atmosres.2021.105950, 2022b.

Zare, A., Fahey, K. M., Sarwar, G., Cohen, R. C., and Pye, H. O. T.: Vapor-Pressure Pathways Initiate but Hydrolysis Products Dominate the Aerosol Estimated from Organic Nitrates, ACS Earth Sp. Chem.,

3, 1426–1437, https://doi.org/10.1021/acsearthspacechem.9b00067, 2019.

Zhang, X., Cappa, C. D., Jathar, S. H., McVay, R. C., Ensberg, J. J., Kleeman, M. J., and Seinfeld, J. H.: Influence of vapor wall loss in laboratory chambers on yields of secondary organic aerosol, Proc. Natl. Acad. Sci. U. S. A., 111, 5802–5807, https://doi.org/10.1073/pnas.1404727111, 2014.

Zhang, X., Schwantes, R. H., McVay, R. C., Lignell, H., Coggon, M. M., Flagan, R. C., and Seinfeld, J. H.: Vapor wall deposition in Teflon chambers, Atmos. Chem. Phys., 15, 4197–4214, https://doi.org/10.5194/acp-15-4197-2015, 2015.

Zhang, Y., Pei, C., Zhang, J., Cheng, C., Lian, X., Chen, M., Huang, B., Fu, Z., Zhou, Z., and Li, M.: Detection of polycyclic aromatic hydrocarbons using a high performance-single particle aerosol mass spectrometer, J. Environ. Sci. (China), 124, 806–822, https://doi.org/10.1016/j.jes.2022.02.003, 2023.

Zhang, Z., Wang, H., Chen, D., Li, Q., Thai, P., Gong, D., Li, Y., Zhang, C., Gu, Y., Zhou, L., Morawska, L., and Wang, B.: Emission characteristics of volatile organic compounds and their secondary organic aerosol formation potentials from a petroleum refinery in Pearl River Delta, China, Sci. Total Environ., 584–585, 1162–1174, https://doi.org/10.1016/j.scitotenv.2017.01.179, 2017.

867 **Table 1**. Summary of experimental conditions in this study.

Exp	RH	Seed	ΔHC (ppb)[b]	ΔHC (μg m^{-3})[b]	N_2O_5 (ppb)	HC:N_2O_5 Ratio	ΔM_O (μg m^{-3})[c,d]	SOA Mass yield (%)[f]
1	<3%	AS[a]	9.5 ± 0.3	40.7 ± 1.4	20	1:2	1.9 ± 0.1	4.5 ± 0.3
2	<3%	AS	15.6 ± 0.5	67.1 ± 2.3	36	1:2	5.4 ± 0.3	8.1 ± 0.6
3	<3%	AS	18.0 ± 0.6	77.6 ± 2.7	40	1:2	6.8 ± 0.4	8.6 ± 0.6
4	<3%	AS	28.4 ± 1.0	122.0 ± 4.3	60	1:2	12.4 ± 0.8	10.1 ± 0.7
5	<3%	AS	48.2 ± 1.7	207.2 ± 7.3	100	1:2	26.1 ± 1.7	12.6 ± 0.9
6	<3%	AS	80.1 ± 2.8	344.4 ± 12.1	160	1:2	48.5 ± 3.1	14.1 ± 1.0
7	<3%	AS	99.1 ± 3.5	426.0 ± 14.9	200	1:2	67.0 ± 4.3	15.7 ± 1.1
8	<3%	AS	155.2 ± 5.4	667.5 ± 23.4	310	1:2	107.4 ± 6.9	16.1 ± 1.2
9	<3%	None	18.2 ± 0.6	78.3 ± 2.7	40	1:2	0.6 ± 0.04	0.8 ± 0.06
10	<3%	None	100.4 ± 3.5	431.8 ± 15.1	200	1:2	47.6 ± 3.0	11.0 ± 0.8
11	50%	AS	17.3 ± 0.6	74.5 ± 2.6	40	1:2	/[e]	/[e]
12	70%	AS	15.8 ± 0.5	67.8 ± 2.4	40	1:2	/[e]	/[e]

[a.] Ammonium sulfate. [b.] Uncertainties in hydrocarbon concentrations are calculated from 3.5% uncertainty in hydrocarbon concentration measured by GC-FID. [c.] Density is 1.35 ± 0.05 g m^{-3}, calculated from the comparison of HR-ToF-AMS and SMPS size distribution data. [d.] Uncertainties in aerosol mass loading are estimated based on uncertainty in aerosol volume concentration measured by the SMPS (5.3%) and uncertainty in SOA density (3.5%). [e.] These numbers are not reported because the density of SOA in humid experiments is not available. [f.] Uncertainties in SOA mass yields are propagated from the uncertainty associated with hydrocarbon concentration and aerosol mass loading.

868

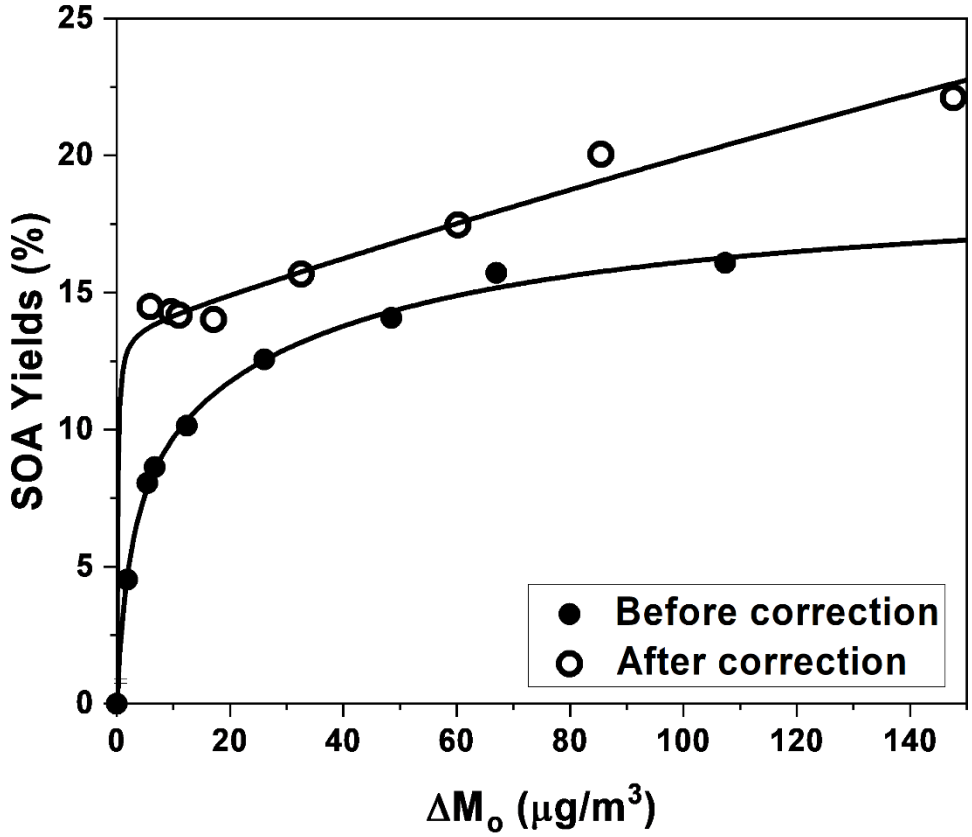

869

870 **Figure 1.** SOA yield data and yield curves for styrene+NO_3 oxidation with and without vapor wall loss
871 correction.

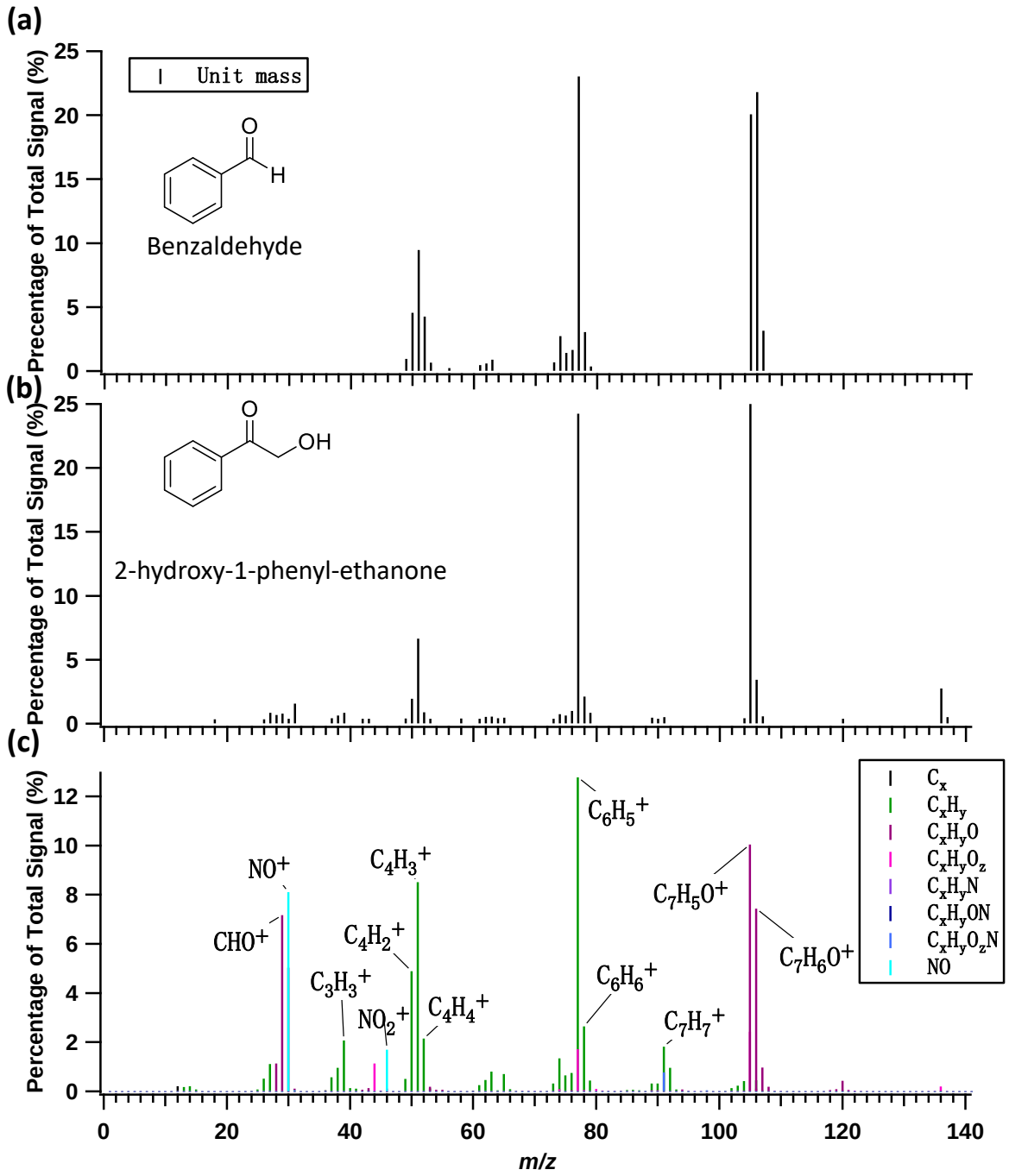

872
873 **Figure 2**. Comparison between the National Institute of Standards and Technology (NIST) mass spectra of
874 (a) benzaldehyde; (b) 2-hydroxy-1-phenyl ethenone; and (c) the HR-ToF-AMS mass spectrum (in integer
875 *m/z*) of SOA from styrene+NO_3 oxidation. The chemical structures for benzaldehyde and 2-hydroxy-1-
876 phenyl ethenone are shown in (a) and (b).

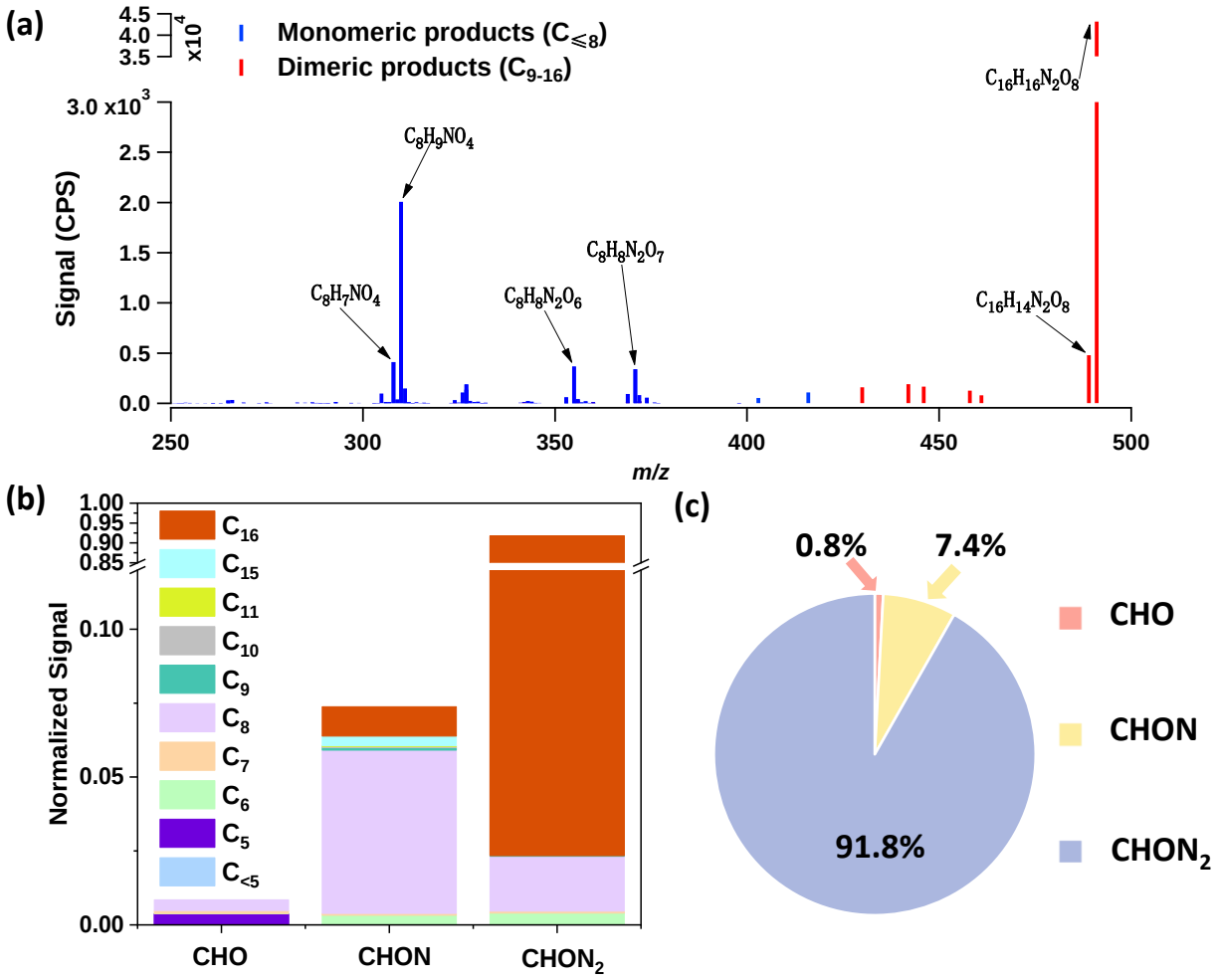

Figure 3. (a) A typical FIGAERO-CIMS mass spectrum of SOA from styrene+NO_3 oxidation (Exp. 7). The sticks are colored to distinguish between monomeric and dimeric products, as indicated in the legend. Prominent masses are labeled with the corresponding chemical formulae without an iodide ion. Only *m/z* 250-500 are shown here, there are no specific major products before *m/z* 250 except I^- and HNO_3I^- ; (b) SOA product distribution, categorized by molecule types: CHO, CHON, and $CHON_2$. Each category is further subdivided by carbon number; (c) The pie chart illustrates the relative percentage contributions of CHO, CHON, and $CHON_2$.

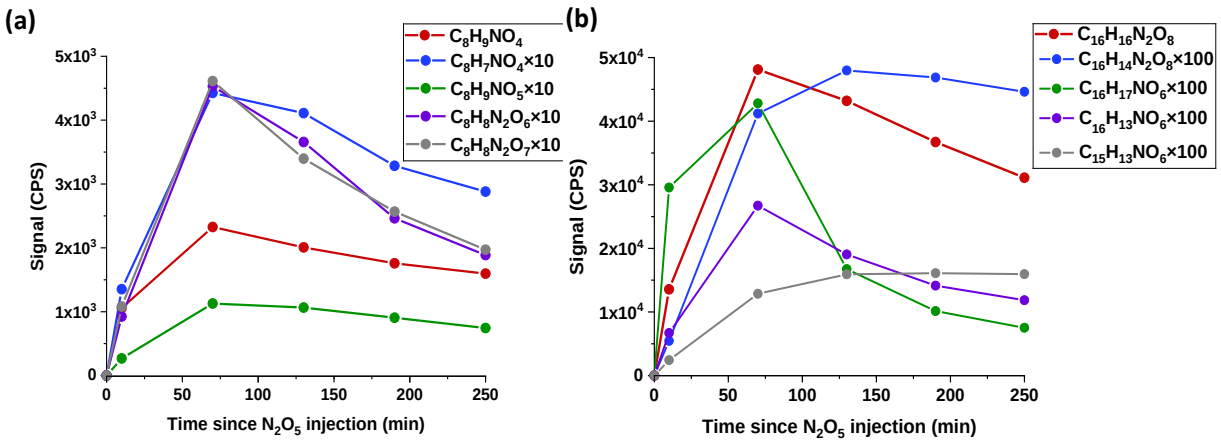

885
886 **Figure 4.** The time series of major particle-phase products from styrene+NO_3 oxidation measured by
887 FIGAERO-CIMS (Exp. 7), including: (a) monomeric styrene ONs; and (b) dimeric styrene ONs.

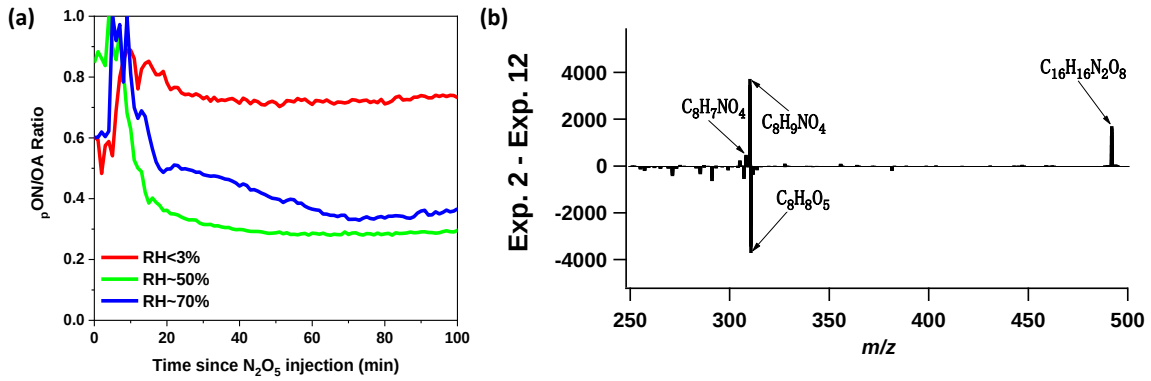

888

889 **Figure 5. (a)** Time series data of the ratio of particulate ONs ($_pON$) to total organic aerosols (OA) in
890 Exp. 2 (RH<3%), Exp. 11 (RH~50%), and Exp. 12 (RH~70%); (b) FIGAERO-CIMS difference mass
891 spectrum of SOA: Exp. 2 (RH<3%) minus Exp. 12 (RH~70%). Prominent masses are labeled with the
892 corresponding chemical formulae without an iodide ion.

893

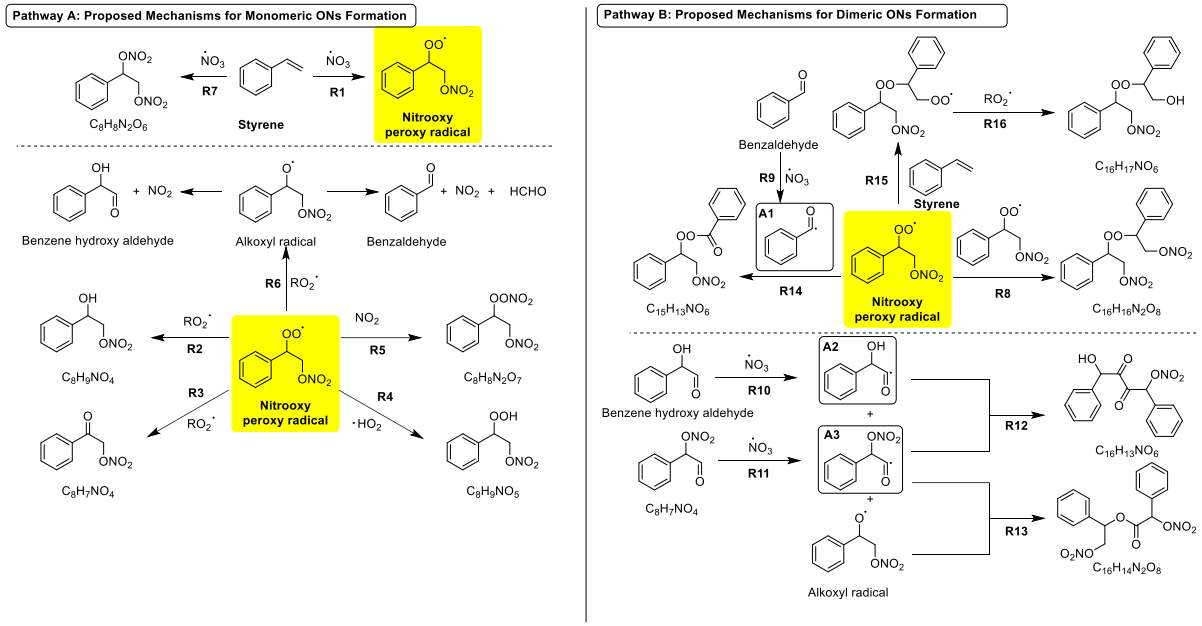

Figure 6. The proposed formation mechanisms for the major particle-phase products resulting from styrene+NO_3 oxidation includes two distinct pathways: Pathway A is the proposed formation pathway for monomeric ON products. Pathway B is the proposed formation pathway for dimeric ON products. Radicals A1, A2, and A3 are highlighted in the boxes as the major products resulting from the reaction between aldehydes and NO_3 radicals. The nitrooxy peroxy radical is highlighted in yellow as the major RO_2 in mechanisms. All chemical structures in the formation mechanisms are proposed based on the molecular formulas of the detected species (shown beneath the structures) or fragments measured by HR-ToF-AMS and require validation through further experiments or theoretical calculations.